Received: 2 July 2019 | Revised: 4 September 2019 | Accepted: 10 September 2019

DOI: 10.1002/aoc.5269

WILEY Applied Organometallic Chemistry

FULL PAPER

Syntheses, characterizations, crystal structures, DFT/TD-DFT, luminescence behaviors and cytotoxic effect of bicompartmental Zn (II)-dicyanamide Schiff base coordination polymers: An approach to apoptosis, autophagy and necrosis type classical cell death

Dhrubajyoti Majumdar[1,2] | **Yashika Agrawal**[3] | **Renjith Thomas**[4] | **Zakir Ullah**[5,6] | **Manas K. Santra**[3] | **Sourav Das**[7] | **Tapan K. Pal**[8] | **Kalipada Bankura**[1] | **Dipankar Mishra**[1]

[1]Department of Chemistry, Tamralipta Mahavidyalaya, Tamluk 721636, West Bengal, India

[2]Department of Applied Chemistry, Indian Institute of Technology (Indian School of Mines), Dhanbad, Jharkhand 826004, India

[3]National Center for Cell Science, Pune 411007, Maharashtra, India

[4]Department of Chemistry, St Berchmans College (Autonomous), Changanassery, Kerala 686101, India

[5]Department of Chemistry, Korea Advanced Institute of Science and Technology (KAIST), Daejeon 34141, Republic of Korea

[6]Center for Catalytic Hydrocarbon Functionalization, Institute for Basic Science (IBS), Daejeon 34141, Republic of Korea

[7]Department of Chemistry, Institute of Infrastructure Technology Research and Management, Ahmedabad 380026, Gujarat, India

[8]School of Liberal Studies, Pandit Deendayal Petroleum University, Gandhinagar 382421, India

Correspondence
Dipankar Mishra, Department of Chemistry, Tamralipta Mahavidyalaya, Tamluk-721636, West Bengal, India.
Email: dmishra.ic@gmail.com

Two new Zn (II)-dicyanamide (dca) 1-D chain coordination polymers (CPs), $[Zn\ (L^{OMe})(\mu_1\text{-dca})(\mu_{1,5}\text{-dca})]_n$ **(1)** and $[Zn\ (L^{OEt})(\mu_1\text{-dca})(\mu_{1,5}\text{-dca})]_n$ **(2)** have been successfully synthesized from bicompartmental Schiff base ligands N,N′-Bis(3-methoxysalicylidenimino)-1,3-diaminopropane (H_2L^{OMe}), N,N′-Bis(3-ethoxysalicylidenimino)-1,3-diaminoproane (H_2L^{OEt}) respectively and structurally characterized using various spectroscopic protocols like ^{1}H NMR, IR, Raman, UV–Vis, fluorescence as well as elemental analysis, TGA, PXRD and SCXRD studies. X-ray single crystal study revealed that both the complexes have two different geometrical arrangement of Zn metal centres with distorted square pyramidal Zn(2) and trigonal prismatic geometry Zn(1). Ab-initio DFT (Density functional theory) has been executed at B3LYP (Becke, 3-parameter, Lee-Yang-Parr) using DGDVP (Diffuse gradient double valence polarised) basis set to explain FMO (Frontier molecular orbital), TD-DFT (Time-dependent density functional theory) and photovoltaic efficiency in Dye Sensitized Solar Cell (DSSC). Hirshfeld surface (HS) and 2D fingerprint plot analyses are shed more light on the non-covalent supramolecular interactions. The steady state and time-resolved fluorescence measurements have been conducted in DMSO and solid-state. CPs exhibited bi-exponential decay in DMSO as well as solid-state where fluorescence behaviors are mainly intra-ligand ($\pi \rightarrow \pi^*$) in nature with lifetimes in the range (1.11–1.06 ns). In particular, in vitro cytotoxic activities were evaluated towards MCF7 (breast cancer) cell line, MDA-MB-231 (breast carcinoma) cell line and MCF10A (breast epithelial) cell line using MTT assay. CP**1** had lower cytotoxic effect against MCF7 (20 μM), MDA-MB-231 (15 μM) cell lines in comparison with cisplatin (42.2 ± 8, 128.2 ± 7 μM). CP**1** induced classical cell death apoptosis, autophagy and necrosis. Lower

Sourav Das, Department of Chemistry, Institute of Infrastucture Technology Research and Management, Near Khokhara Circle, Maninagar East, Ahmedabad-380026, Gujarat, India.
Email: d.sourav245@gmail.com

Funding information
UGC, New Delhi, Grant/Award Number: F.PSW-232/15-16(ERO

IC_{50} value of CP**1** against MDA-MB-231 cell line provide new insights in the development of cancer therapeutics.

Highlights

- Two new Zn(II)-dicyanamide CPs were synthesized and characterized
- X-ray Crystal structures of Zn(II)-CPs were determined
- DFT, TD-DFT and luminescence behaviors have been explored
- Zn(II)-CPs show noteworthy cytotoxic activity against breast cancer cell lines
- Apoptosis, autophagy and necrosis type classical cell death phenomenon was explained

KEYWORDS
cytotoxic, DFT, dicyanamide, photoluminescence, Zn (II)

1 | INTRODUCTION

Over the last few years, design and synthesis of coordination polymers (CPs) of group 12 metal ions have been attracted tremendous attention not only of their novel molecular architectures and topological networks[1–3] but also their blooming field of applications in luminescence,[4–7] chemical sensors,[8–10] antibacterial and anti-biofilm,[11–14] anti-proliferative,[15] organic light emitting diode (OLED).[16–19] Moreover, recently zinc complexes can be used as the photosensitizer in DSSC.[16–19] *Ortho* vanillin derived Schiff base platforms have always excellent coordinating ability with group 12 metal ions to function as sequential multidentate bridging blocks and thus enable to synthesize novel CPs embedded with supramolecular chemistry which flourishing their new potential applications.[20–22] Under such consideration, we have ventured to explore *Ortho* vanillin derived two popular Schiff base ligands (H_2L^{OMe}/H_2L^{OEt}), Zn (II)-dicyanamide CPs to searched for its novel applications. In human body, Zn (II) is the 2nd most important abundant metal ions after iron due to its steady involvement of several biochemical applications.[23,24] Zinc metal ions can induce Alzheimer's disease, Parkinson's disease[25,26] on account of its concentration abnormality in human body. From biological standpoint it constructs many active sites of hydrolytic enzymes and function as Lewis catalyst.[27,28] Pseudo-halides linked Zn (II) or M (II)-Schiff base complexes [where M (II) other transition metal ions] have always excellent bioactivity owing to the presence of azomethine linkage and active metal centres.[29,30] Anticancer properties of Schiff bases enhanced many times after chelated with Zn (II)/M (II) metal ions which can be well explained on the basis of popular "Overtone's concept" and "chelation theory".[31–35] In 21st century, Cancer is the most fatal disease in both developing and developed countries globally.[31–35] High levels of Zn^{2+} ions inhibit growth of mammalian cells severely[31–35] and increasing exposure of such metal ions induce a typical, caspase-independent form of apoptosis.[31–35] A recent study report has clearly shown that this property can be used to kill cancer cells selectively.[31–35]Therefore, to overcome these fatal diseases researcher in coordination chemistry domain always try to synthetically design novel anticancer drugs with d^{10} metal ions in presence of Schiff base ligands and flexible pseudo-halide anions.[31–37]

Due to our long-standing relationship with *ortho* vanillin derived bicompartmental Schiff base ligands, our research group has already reported Zn (II)/Cd (II) complexes photoluminescence, DFT/TD-DFT, in vitro antibacterial and anti-biofilm properties vividly. The outcome of previous research works is that pseudo-halides linked metal complexes exhibit good photophysical, antimicrobial and anti-biofilm properties[11–14,38–42] but no exiguous number of studies of photovoltaic efficiency in Dye Sensitized Solar Cell (DSSC) using TD-DFT, cytotoxic effect, apoptosis, autophagy and necrosis type classical cell death. Zn (II) metal ions always have wide spectrum of flexible geometry due to its d^{10} configuration and zero crystal field stabilization energy value (CFSE).[43–47]Therefore, the key factors for novel syntheses of Zn (II)-CPs are always careful selection of organic Schiff base ligands in conjunction with pseudo-halide anions.[48] In this juncture, flexible dicyanamide, a larger pseudo-halide ion-rod is under active consideration since it exhibits versatile coordination motifs to reinforce the CPs formation.[49–55] Most of the dicyanamide complexes, $\mu_{1,5}$-dca bridging mode is popular and common whereas terminal coordination motif is rare due to its long chain length and negative charge delocalization over the symmetrical molecule.[56,57] Herein a dual

combination of terminal along with $\mu_{1,5}$-dca enabled 1-D chain CPs have been presented.

In this article, we report syntheses, characterizations, single crystal structures, DFT/TD-DFT, photophysical and antiproliferative activities of **1**–**2**. The thermal stabilities of metal–organic frameworks have been investigated by TGA. In addition, apoptosis, autophagy and necrosis type classical cell death phenomena were investigated in detail.

2 | EXPERIMENTAL

2.1 | Materials and instrumentation

All research chemicals and solvents were of reagent grade and used as received without further purification. Zn $(OAc)_2.2H_2O$, Sodium dicyanamide, o-vanillin and 1,3-diaminopropane were purchased from Sigma Aldrich Company, St. Louis, Missouri, USA. The chemicals MTT and Propidium Iodide were also purchased from Sigma Aldrich Company, St. Louis, Missouri, USA. The antibodies against pMEK (sc7995), MEK (sc43612), pERK (sc16982), ERK (K23-sc94), BAX (sc23959), BCL2 (sc7382), Caspase 8 (sc70501), Caspase 9 (sc56073), PARP (sc56198), mTOR (sc1549), Beclin (sc48341), p62 (sc28359), Goat anti-rabbit IgG (sc-2004) and Goat anti-mouse IgG (sc-2005) were obtained from Santa Cruz Biotechnology. AKT (9272), pAKT-473 (4058), pAKT-308 (9275), PUMA (4976), p-mTOR (2974), pS6K (9205) and LC3B (27758) were obtained from Cell Signaling. Antibody against Alpha-Tubulin (T5168) was obtained from Sigma.

Elemental analyses were performed on a Perkin-Elmer 2400 CHN elemental analyzer. FT-IR and Raman spectra were recorded as KBr pellets (4000–400 cm^{-1}) by using Perkin–Elmer spectrum RX 1 and BRUKER RFS 27 (4000–50 cm^{-1}). ^1H NMR spectra of ligands and CPs were recorded on a Bruker 300 MHz FT-NMR spectrometer using trimethylsilane as internal standard in DMSO solvent. Energy dispersive X ray (EDX) experiments was performed on EDAX OXFORD XMX N (model) using Tungsten filament. UV–Visible spectra (200–1100 nm) were determined using Hitachi model U-3501 spectrophotometer. Fluorescence spectra for Schiff base ligands and CPs in DMSO solvent (spectroscopic grade) were measured by using Perkin-Elmer LS50B Spectrofluorometer model at room temperature (298 K). Fluorescence lifetime measurements were recorded by using JOBIN-VYON M/S Fluorimeter. CPs fluorescence lifetime were determined using Equation S1. Thermogravimetric analyses (TGA) were carried out on a TGA-5OH analyzer from ambient temperature to 1000 °C at a temperature rate of 30 °C/min in a flowing 10 ml/min under environment of nitrogen atmosphere using a platinum cell. Powder X-ray diffraction measurements were carried out by BRUKER AXS, GERMANY X-ray diffractometer model using Cu Kα-1

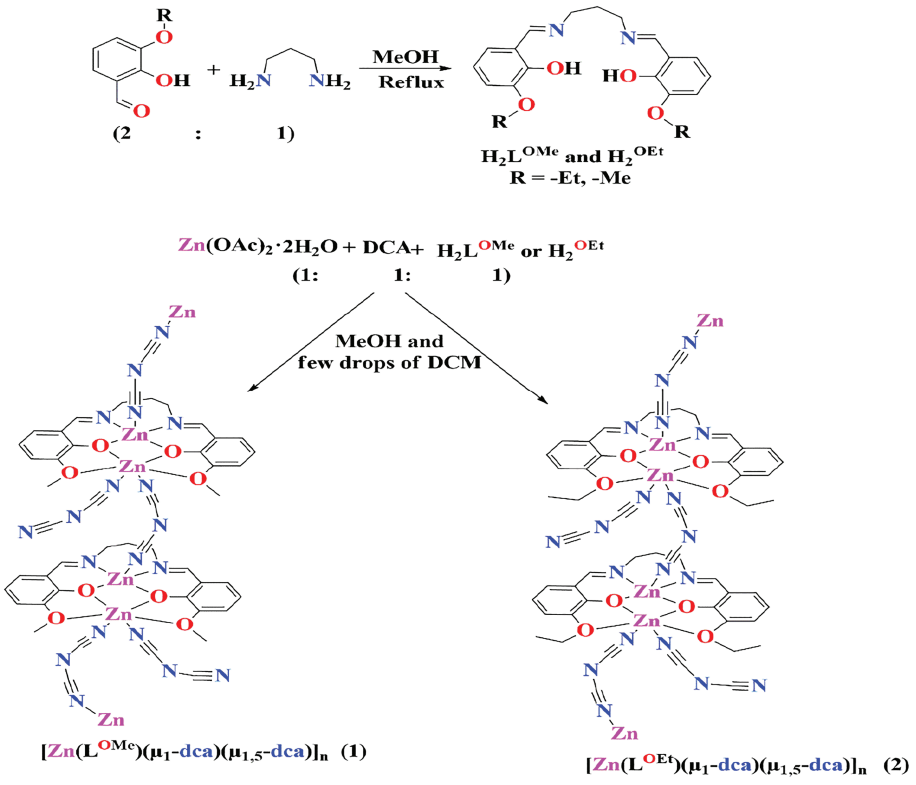

SCHEME 1 Synthetic schemes for Schiff base platforms and CP**1**-CP**2**

radiation. Quantum yield (Φ) have been determined using Equation (1) where quinine sulphate is used as secondary standard (Φ = 0.57 in water).[58]

$$\frac{\Phi_S}{\Phi_R} = \frac{A_S}{A_R} \times \frac{(Abs)_R}{(Abs)_S} \times \frac{n_S^2}{n_R^2} \quad (1)$$

According to Equation (1), A terms denote the fluorescence area under the curve; Abs denotes absorbance; n is the refractive index of the medium; Φ is the fluorescence quantum yield; and subscripts S and R denote parameters for the studied sample and reference respectively.

2.2 | Syntheses of Schiff base ligands

Two Schiff base ligands were synthesized in similar ways as previously literature reported method (Scheme 1).[59] Briefly, ligands (H_2L^{OMe}/H_2L^{OEt}) are 1:2 condensation product of 1,3-diaminopropane (0.0371 g, 0.5 mmol) with 3-methoxy-2-hydroxybenzaldehyde (0.152 g, 1 mmol) and 3-ethoxy-2-hydroxybenzaldehyde (0.166 g, 1 mmol) in (50 ml) methanol at 70 °C for 1 hr. The yellow or orange colored ligand separated out upon cooling the solution which was collected and dried. N, N′-Bis(3-methoxysalicylidenimino)-1,3-diaminopropane (H_2L^{OMe}): Yield: (90%), Anal. Calc. for $C_{19}H_{22}N_2O_4$: C, 66.65; H, 6.48; N, 8.18 Found: C, 66.71; H, 6.42; N, 8.08%. IR (KBr cm^{-1}) selected bands: ν(C═N), 1640, ν(C-$O_{phenolic}$) 1254, ν(O-H) 3449, UV–Vis (λ_{max}/nm): 330 nm.

N, N′-Bis(3-ethoxysalicylidenimino)-1,3-diaminopropane (H_2L^{OEt}): Yield: (88%), Anal. Calc. for $C_{21}H_{26}N_2O_4$: C, 68.09; H, 7.07; N, 7.56 Found: C, 67.18; H, 7.12; N, 7.90%. IR (KBr cm^{-1}) selected bands: ν(C═N), 1641, ν(C-$O_{phenolic}$) 1256, ν(O-H) 3448, UV–Vis (λ_{max}/nm): 340 nm.

2.3 | Synthesis of CPs

2.3.1 | $[Zn(L^{OMe})(\mu_1\text{-dca})(\mu_{1,5}\text{-dca})]_n$ (1)

To the methanolic solution (25 ml) of zinc acetate dihydrate (0.2195 g, 1 mmol), Schiff base ligand (H_2L^{OMe}) solution was added drop by drop and the resulting solution was stirred for 15 mins. An aqueous methanolic solution (5 ml) of sodium dicyanamide (0.0891 g, 1 mmol) was then added. The overall reaction mixture was refluxed for 25 min at 60 °C. 10 ml of Dichloromethane (DCM) were also added into the reaction mixture. The stirring was continued for about 3 hr. Finally, the light-yellow filtrate was kept for crystallization by slow evaporation at room temperature. Single crystal, suitable for X-ray diffraction were obtained after 10 days on slow evaporation of the solution in open atmosphere. Crystals were isolated by filtration and air dried. Yield: 0.458 g, Anal. Calc. for $C_{23}H_{20}N_8O_4Zn_2$: C, 45.79; H, 3.34; N, 18.58. Found: C, 45.75; H, 3.29; N, 18.49%. IR (KBr cm^{-1}) selected bands: ν(C═N), 1620 vs, ν(C ≡ N), 2290 s, 2180 s, 2090 m, FT-Raman (cm^{-1}) selected bands: ν(C═N), 1628 vs, ν(C ≡ N), 2274 vs, 2235 vs, 2169 s, UV–Vis λ_{max} (DMSO): 276 nm, 358 nm.

2.3.2 | $[Zn(L^{OEt})(\mu_1\text{-dca})(\mu_{1,5}\text{-dca})]_n$ (2)

CP**2** was prepared by adopting similar procedure as **1** except Schiff base solution used is (H_2L^{OEt}). Yield: 0.460 g, Anal. Calc. for $C_{25}H_{24}N_8O_4Zn_2$: C, 45.56; H, 3.83; N, 17.75 Found: C, 45.51; H, 3.78; N, 17.70%. IR (KBr cm^{-1}) selected bands: ν(C═N), 1620 vs, ν(C ≡ N), 2300 s, 2210 s, 2170 s, FT-Raman (cm^{-1}) selected bands: ν(C═N), 1631 vs, ν(C ≡ N), 2264 vs, 2236 vs, 2182 m, UV–Vis λ_{max} (DMSO): 275 nm, 356 nm.

2.4 | X-ray crystallography

The good quality single crystals for CPs were selected and mounted on a Bruker *SMART* CCD[60] diffractometer using Mo K_α radiation at $\lambda = 0.71073$ Å. Crystal data collection purpose different common programs were operated e.g. *SMART* program used for collecting frames of data, indexing reflections, and determining lattice parameters, *SAINT*[61] for integration of the intensity of reflections and scaling, *SADAB*[62] for absorption correction and popular SHELXTL for space group and structure determination and least-squares refinements on F^2. The crystal structure was fully solved and refined by full-matrix least-squares methods against F^2 using the common program *SHELXL*[63] and *Olex-2* software.[64] All the non-hydrogen atoms were refined with anisotropic displacement parameters. All H atoms were generated geometrically, and positions were fixed at calculated positions and refined isotopically. Crystallographic diagrams were constructed using latest Diamond software.[65] The selected crystallographic data, experimental conditions and relevant structural refinements for CPs were clearly summarized in Table 1. Crystallographic data (excluding structure factors) for CP**1**-CP**2** have been deposited with the Cambridge Crystallographic Data Centre as supplementary publication numbers CCDC 1901797–1 901 798.

2.5 | DFT calculations

CPs are subjected to high level computational studies after optimizing the geometry with B3LYP functional and the Split Valance Polarisation (DGDVP) basis set,

TABLE 1 Crystallographic parameters for CP**1** and CP**2**

Formula	$C_{23}H_{20}N_8O_4Zn_2$ (1)	$C_{25}H_{24}N_8O_4Zn_2$ (2)
M/g	603.21	631.26
Crystal system	Monoclinic	Orthorhombic
Space group	$P2_1/n$	$P2_12_12_1$
a/Å	8.805(2)	9.2767(8)
b/Å	15.613(4)	12.2635(10)
c/Å	18.541(5)	23.804(2)
α (°)	90	90
β (°)	90.068(9)	90
γ (°)	90	90
V/Å^3	2534.5(12)	2708.1(4)
Z	4	4
ρ_c/g cm^{-3}	1.581	1.548
μ/mm^{-1}	1.939	1.818
$F(000)$	1224	1288
Cryst size (mm^3)	0.052× 0.031 × 0.022	0.2× 0.2 × 0.1
θ range (deg)	0.993	0.996
Limiting indices	-10 ≤ h ≤ 10	−11 ≤ h ≤ 11
	−18 ≤ k ≤ 18	−14 ≤ k ≤ 14
	−21 ≤ l ≤ 21	−16 ≤ l ≤ 28
Reflns collected	29 021	20 195
Ind reflns	4466[R_{int} = 0.049, R_{sigma} = 0.0340]	4744[R_{int} = 0.0320, R_{sigma} = 0.0318]
Completeness to θ (%)	0.993	0.996
Refinement method	Full-matrix-block least-squares on F^2	Full-matrix-block least-squares on F^2
Data/restraints/parameters	4466/18/324	4744/0/354
Goodness-of-fit on F^2	1.037	1.023
Final R indices	R_1 = 0.0431	R_1 = 0.0242
[$I > 2\theta(I)$]	wR_2 = 0.1018	wR_2 = 0.0625
R indices (all data)	R_1 = 0.0662	R_1 = 0.0281
	wR_2 = 0.1132	wR_2 = 0.0646
Largest diff. Peak and hole (e ·Å^{-3})	1.060 and − 0.691	0.361and −0.321

which is among Karlsruhe basis sets. We commonly used popular Gaussian 09 W[66–68] for simulations and Gauss View 5.0[66–68] for visualizations. Frequency calculations are performed to make sure that there are no imaginary frequencies and the simulated structure refers to a minimum energy conformation. Electronic transition, being a time resolved process, the electronic spectra can be modelled computationally by TD-DFT using new hybrid exchange–correlation functional using the Coulomb-attenuating method called CAM-B3LYP functional using the same basis set used for geometry optimizations. PCM model is used to create a solvent atmosphere of the DMSO solvent. HS and 2D fingerprint plots were generated using Crystal Explorer 17[66–68] using cif files for CPs obtained as a result of single crystal X-ray diffraction analysis. HS were calculated with B3LYP level functional and 6-31G(d) basis set using the TONTO *Abinitio* and DFT code fixed within the Crystal Explorer 17.

2.6 | Experimental of cytotoxicity

2.6.1 | Cell culture

CPs including synthesized Schiff base ligands were dissolved in DMSO to prepare 25 mM stock solutions. Further

dilutions were also made in DMSO. During treatment, the final concentration of DMSO was maintained <0.1%. Breast epithelial cell line MCF10A was grown in DMEM/F12 (Dulbecco's Modified Eagle Medium) supplemented with 5% horse serum, 20 ng/ml EGF, 0.5 mg/ml hydrocortisone, 100 ng/ml cholera toxin and 10 μg/ml insulin. Breast cancer cell line MCF7 was grown in DMEM (high glucose) (Dulbecco's Modified Eagle Medium) and MDA-MB-231 was grown in RPMI as monolayer with 10% FBS (Foetal Bovine Serum) 100 U/ml penicillin and 100 μg/ml streptomycin. All the cell lines were grown at 37°C in a humid, 5% CO_2 regulated incubator.

2.6.2 | Growth inhibition by MTT assay

The cytotoxic effect of CP**s** and ligands was determined using MTT (3-[4, 5 dimethylthiazol-2-yl]-2,5-diphenyltetrazolium bromide) assay as described previously.[69] Briefly, the cells were seeded (3×10^3 cells per well) in 96 well plates. After 24 hrs, cells were treated with varying concentrations (0–100 μM) of respective compounds for 48 hrs in triplicates. After 48 hrs of drug treatment, 20 μL MTT solution (5 mg/ml MTT stock) was added to each well of the 96 well plate and incubated further for 3.5 hrs in humid 5% CO_2 incubator. Media containing MTT solution was then replaced by MTT solvent (4 mM HCl and 0.1% Triton X-100 in iso-propanol), incubated for 15 min at room temperature with gentle shaking to ensure the complete dissolution of Formazan. Absorbance was measured at 570 nm using a Thermo Scientific Multiskan GO Elisa plate reader. All experiments were carried out three times in triplicate and the percentage of viable cells was calculated as the mean with respect to the vehicle treated cells.

2.6.3 | S-cell cycle analysis by fluorescence activated cell sorting (FACS)

The cells were treated with different concentrations of CPs for 48 hours and then collected for FACS analysis**.** Propidium Iodide staining was performed for the total DNA content of the cells as described previously.[70] Briefly, the cells were washed with phosphate buffer saline (PBS), trypsinized and centrifuged at 1500xg for 3 mins at 4 °C. The cells were then fixed and permeabilized using 900 μL of 95% chilled ethanol which was added drop wise along with continuous vertexing and cells were then stored overnight at 4 °C. The fixed cells were centrifuged at 1500 x g for 3 mins and washed twice with PBS. The cells were dissolved and stained with 500 μL staining solution (900 μL PBS, 2 mM $MgCl_2$, 50 μL PI stock solution (5 mg/ml PI in PBS), 50 μL RNase A (1 mg/ml RNase A) (Sigma)) and incubated at 37 °C for 20 mins. Cells were then passed through cell strainers and proceeded for FACS acquisition on BD FACS Cali bur. The raw data was then analyzed using Cell Quest pro software.

2.6.4 | Colony formation assay

Colony formation assay was performed to check the long-term growth of cells upon treatment of the drug as described previously.[70] Briefly, MCF7 and MDA-MB-231 cells were seeded in 35 mm plates (5×10^3 cells) and were grown in DMEM (Dulbecco's Modified Eagle Medium) and RPMI media supplemented with 10% FBS in 5% CO_2 at 37 °C, respectively. After 48–72 hrs of growth, MCF7 cells were treated with 20 μM of CP**1** and MDA-MB-231 cells were treated with 15 μM of CP**1**. Media was changed after 48 hrs of treatment and cells were allowed to form colonies for 2 weeks. Then, the cells were fixed with 3.7% formaldehyde solution followed by staining with 0.5% crystal violet for 15 mins. Stained cells were then washed with PBS three times with gentle rocking at room temperature to remove the residual crystal violet solution. The images were obtained using the Amersham Imager 600 (GE Healthcare Lifesciences) and the experiment was repeated three times.

2.6.5 | Cell lysate preparation and immunoblotting

Cells were harvested and washed twice with ice-cold PBS. Cells were then lysed with whole cell lysis buffer (50 mM Tris pH 7.4, 200 mM NaCl, 50 mM NaF, 1 mM Na_3VO_4, 0.5% Triton X-100 and protease inhibitor cocktail) in ice for 30 mins as described previously.[70] Cell lysates were centrifuged at high speed (16 000xg) and supernatants were transferred to new tubes. Protein concentration was measured by Bradford method using bovine serum albumin as a standard.[71] The protein samples were resolved using SDS-PAGE with Tris-Glycine (25 mM Tris, 192 mM Glycine) running buffer containing 0.1% SDS. Separated proteins were transferred onto the PVDF membrane with transfer buffer (Tris-Glycine and 20% Methanol). Membrane was incubated with indicated primary antibodies overnight at 4 °C. The primary antibody was then removed, and blots were incubated for 1 hr with secondary antibody. Blots were then developed by chemiluminescence method.

2.6.6 | DNA fragmentation assay

The assay was performed as per the protocol described previously.[72] Briefly, the cells were harvested, washed

with ice-cold PBS and lysed in NP40 lysis buffer (20 mM EDTA, 50 mM Tris-Cl, pH 7.5 and 1% NP40) for 10 seconds in ice. Cell lysates were centrifuged at 1600xg for 5 mins and the supernatant was collected. The pellet was resuspended in NP40 lysis buffer and centrifuged to obtain the second batch of supernatant. Both the supernatants were mixed and SDS (final concentration 1%) was added. RNase A was added to the mixture (final concentration 5 μg/μl) and incubated at 56 °C for 2 hr. Proteinase K (final concentration 2.5 μg/μl) was added and the mixture was further incubated for 2 hr and 37 °C. Half volume of ammonium acetate (10 M) was added followed by glycogen. The DNA was precipitated with 2.5 volume of ethanol and incubated at −20 °C overnight. The mix was then centrifuged at 5000xg for 30 mins; pellet was dissolved in gel loading buffer and separated on 3% agarose gel.

3 | RESULTS AND DISCUSSIONS

3.1 | Synthesis

Schiff base ligand platforms were synthesized by the condensation of 1,3-diaminopropane with o-vanillin in MeOH at 1:2 M ratio.[59] Using dicyanamide spacer, CPs derived in a good yields by taking the following procedure where 1:1:1 M ratio of zinc acetate dihydrate, Schiff base (H_2L^{OMe}/H_2L^{OEt}) and sodium dicyanamide [NaN $(CN)_2$] in methanolic solution under stirred condition (Scheme 1). The binding versatile ability of ligands and dicyanamide spacer with metal ions (M^{2+}) are submitted in Scheme S1-S2. The crystalline form of CPs was only isolated from slow evaporation of mixed solvent (CH_3OH-DCM) at room temperature. A close inspection of ligands structure completely divulges that it comprises two

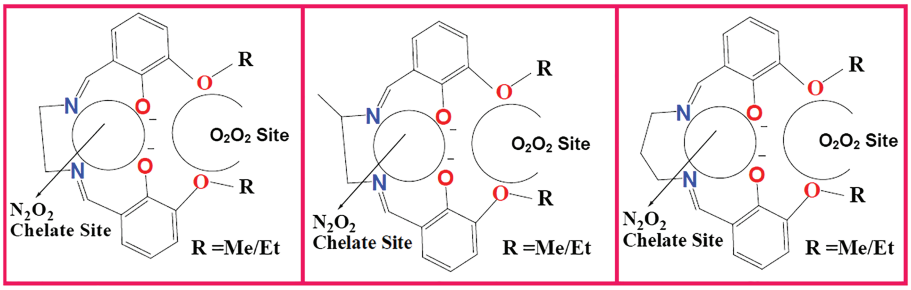

SCHEME 2 Similarities of Ω-shape H_2vanen ligand with other compartmental ligands

TABLE 2 Compartmental ligands coordination features with Zn (II) and dicyanamide anion

Salen-type ligands	Ligands pocket used	Zn (II)-dca complexes/CPs	Ref
1. [N, N′-bis(3-methoxysalicylidenimino)-1,3-diamino propane] [H_2L^{OMe}]	N_2O_2 and O_2O_2	Terminal and $\mu_{1,5}$-dca bridging mode. 1-D CPs	This work
[N, N′-bis(3-ethoxysalicylidenimino)-1,3-damino propane] [H_2L^{OEt}]			
2. N, N′-bis(2-hydroxy-3-methoxybenzylidene) -propane-1, 2-diamine) [H_2L^{OMe}]	N_2O_2 and O_2O_2	Terminal and $\mu_{1,5}$-dca bridging mode. Di-nuclear. Isostructural	11–14
N, N′-bis(2-hydroxy-3-methoxybenzylidene)-propane-1,2 -diamine) [H_2L^{OEt}]			
3. N, N′-ethylene bis(3methoxysalicylaldimine)	N_2O_2 and Ω-shape O_2O_2	Terminal and $\mu_{1,5}$-dca bridging. Zn_4/Zn_3-nuclear neutral metal complexes	56,57
N, N′-ethylene bis(3-ethoxysalicylaldimine)			
[H_2vanen-type ligands]			

imines, two phenols and (-OR) groups. After deprotonation of either $[L^{OMe}]^{2-}$ or $[L^{OEt}]^{2-}$, the N_2O_2 imine-based chelating sites are available to bind M^{2+} ions whereas CPs formation with dicyanamide spacer in presence of zinc metal is still unveiled of research. Apart from, ligands structural platforms are close resemblance with Ω-shape H_2vanen-type or other compartmental ligands (Scheme 2).[11–14,56,57]In this context our research group highlighted the coordination motifs of compartmental ligands with Zn (II)-nodes and dicyanamide spacer (Table 2). The general stoichiometries of CPs have been corroborated thoroughly by the microanalytical results. CPs were yellow coloured solid, non-volatile, stable on prolonged exposure to light and air, insoluble in water and successfully characterized using various spectroscopic protocols like FT-IR, FT-Raman, ^{1}H NMR, UV–Vis along with EDAX, powder X-ray diffraction, TGA, X-ray crystallography and fluorescence spectroscopy.

3.2 | Spectroscopic characterizations

FT-IR spectra of CPs were carefully analyzed and compared with those of the corresponding bicompartmental Schiff base ligands (H_2L^{OMe}/H_2L^{OEt}) and different well-known stretching vibrations are listed in Table 3. Thus, Schiff base formations are characterized by IR, and UV–Vis spectroscopic studies (Figure S1, Figure S2). The characteristic imines (C=N) stretching vibration of two Schiff base ligands are found to be 1640 cm^{-1} and 1641 cm^{-1} respectively. The absence of the N-H stretching band near at 3150–3450 cm^{-1} positively confirmed the condensation of all the primary amine groups. Well defined stretching bands at 3449 and 3448 cm^{-1} in the spectra of two Schiff base ligands are due to O-H stretching which disappeared in Zn (II)-CPs.[73] In CP**1** and CP**2**, IR and FT-Raman (C=N) stretching vibration bands are shifted to 1620 cm^{-1} (for IR) and 1628, 1631 cm^{-1} (for Raman) respectively (Figure S3). The above mention data directly confirmed the coordination of the imine nitrogen atom to the zinc metal centers.[74–76] Dicyanamide anion [N (CN)$_2$]$^-$ showed three sharp characteristic band preferably in the region 2300–2170 cm^{-1}.[77] Two medium intensity bands (at 2290, 2180 cm^{-1} in CP**1** and 2300, 2210 cm^{-1} in CP**2**) and effective strong intensity band (at 2090 cm^{-1} in CP**1** and 2170 cm^{-1} in CP**2**) are indicative of the presence of dicyanamide spacer in the CPs. IR spectra with previously reported Zn (II)-dicyanamide complexes were compared in Table S3. Raman spectral data's (previously reported Zn (II)-dicyanamide complexes) were additionally explore to support the presence of bridging propensity of [N $(CN)_2]^-$ anions (Table S4). Ar-O stretching frequencies of CPs observed near at 1280–1220 $cm^{-1}$and 1300–1250 cm^{-1} which is similar to the previously reported salen-type ligands.[78] UV–Vis spectra (Figure S2) of Schiff bases at 330 and 340 nm are assigned due to $\pi \rightarrow \pi^*$ and $n \rightarrow \pi^*$ type electronic transitions. CPs in DMSO solvent exhibit ligand–based transition at 275 nm, 358 nm and 275 nm, 356 nm (Figure S2) due to $\pi \rightarrow \pi^*$ or $n \rightarrow \pi^*$ type of transitions.[79] Herein no characteristic broad d-d absorption band was assigned in the UV–Vis spectra.

3.3 | ^{1}H NMR spectroscopy

Two Schiff base formations and its effective coordination mode with Zn (II) in CPs has been confirmed by ^{1}H NMR spectroscopic study. The ^{1}H NMR proton numbering scheme of ligands are represented in Scheme 3 and the corresponding NMR spectra of ligands and CPs are clearly submitted in Figure S1A. For free ligands NMR spectra, no broad peak was identified in the region δ

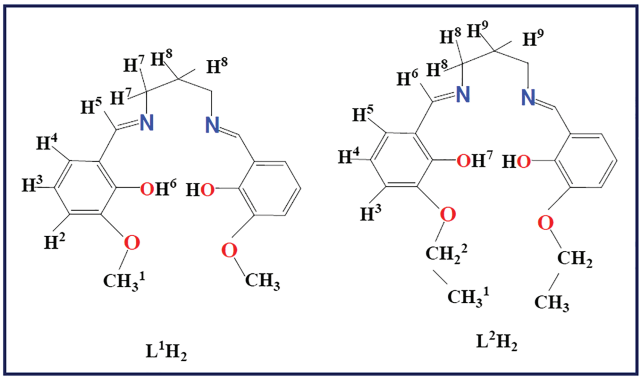

SCHEME 3 ^{1}H NMR proton numbering scheme of Schiff base ligands

TABLE 3 FT-IR spectral data (cm^{-1}) of Schiff base ligands and CPs

Compounds	ν(C=N)	ν(C-$O_{Phenolic}$)	ν(O-H)/H_2O	ν(N-H)	ν (Zn-N)	ν (dca)
(H_2L^{OMe})	1640	1254	3449	3150–3450 absence	-	-
(H_2L^{OEt})	1641	1256	3448	3150–3450 absence	-	-
CP1	1620	1280–1220	-	-	453	2290–2180 s 2090 vs
CP2	1620	1300–1250	-	-	445	2300–2210 s 2170 vs

5.0–8.0 ppm indicating positively the absence of free -NH_2 group function. This situation is further confirmed the formation of Schiff base ligands during condensation process.[80] Ligands aromatic proton peak is assigned in between δ 6.75 and 6.95 ppm. H^5 and H^6 protons are attached to the imino carbon of (H_2L^{OMe}) and (H_2L^{OEt}) are downfield shifted (δ 8.46–8.52 ppm) since these two protons are influenced by the close vicinity of phenolic -OH and imino nitrogen groups. The methylene protons assigned as H^7 for (H_2L^{OMe}) and H^8 for (H_2L^{OEt}) are close vicinity with imino nitrogen, such protons are deshielded and appear as a 2H triplet at δ 3.8–3.9 ppm. Three methylene protons (H^1) since attached to the aromatic oxygen (H_2L^{OMe}**)** appear as a 3H singlet at δ 3.84 ppm whereas for (H_2L^{OEt}) these hydrogens are intervened by a -CH_2 group appear at upper field as a triplet at δ 1.28 ppm. Further, for (H_2L^{OEt}) due to intervening -CH_2 group protons (H^2) appear as upper field quartet at δ 3.97 ppm. This proton character is paramagnetic influenced of the aromatic oxygen. CP**1** and CP**2** was also characterized by ^{1}H NMR spectra. Comparison of ^{1}H NMR spectra of CPs with respect to free Schiff base ligands indicates that the proton signal corresponding to OH group of ligands are completely disappeared in both CPs which may be due to deprotonation. Further, signals of H^3-H^6 are broadened compared to the free ligand (H_2L^{OEt}) possibly due to spin–lattice relaxation caused by paramagnetic impurities in the CPs.[81]

3.4 | EDAX analysis

The weight (%) contribution of the elements of dicyanamide modulated CPs were further confirmed from the EDAX profile analyses. The weight (%) contribution of the elements present in CPs were clearly submitted in Table S5 and the related EDAX profiles are shown in Figure S4. The calculated and EDAX values of CPs are nearly good agreement. Therefore, the empirical formula of CP**1** and CP**2** is formulated as $C_{23}H_{20}N_8O_4Zn_2$ and $C_{25}H_{24}N_8O_4Zn_2$. EDAX profile shows highest peak of only C and thereafter O, Zn which further established the empirical formula of dicyanamide linked zinc metal CPs.

3.5 | Phase purity studies

Powder X-ray diffraction patterns for CPs were recorded at room temperature. The X-ray powder diffraction patterns for CPs were recorded experimentally after small (2θ) scanning from 4^0 to 50^0. The experimental PXRD patterns (Figure S5) of the bulk materials for CPs are similar with the patterns simulated from single X-ray crystal diffraction data (CIF **1** & **2**) obtained from CCDC Mercury software consisting that single crystals and bulk material are the same. Further, results of PXRD study can provide the confirmation of the phase purity of each bulk sample.

4 | SINGLE-CRYSTAL X-RAY DIFFRACTION STUDIES

4.1 | Crystal structure of CP1

Single crystal X ray diffraction study of CP**1** reveals that **1** is a neutral and consist of two crystallographic independent zinc metal ions with the formula [ZnL^{OMe} $(dca)_2$] where, dca = dicyanamide ion. The CP**1** crystallized in the monoclinic space group $P2_1/n$ (Z = 4). In this complex all the metal ions are in full occupancy and charge is balanced by the ligand, $[L^{OMe}]^{2-}$ and the co-ligand, dicyanamide anion. The ORTEP diagram of asymmetric unit of CP**1** is given in the Figure 1 whereas selected bond angle and bond length parameters of CPs are given in the Table S1-S2. From structural point of view of (H_2L^{OMe}), it

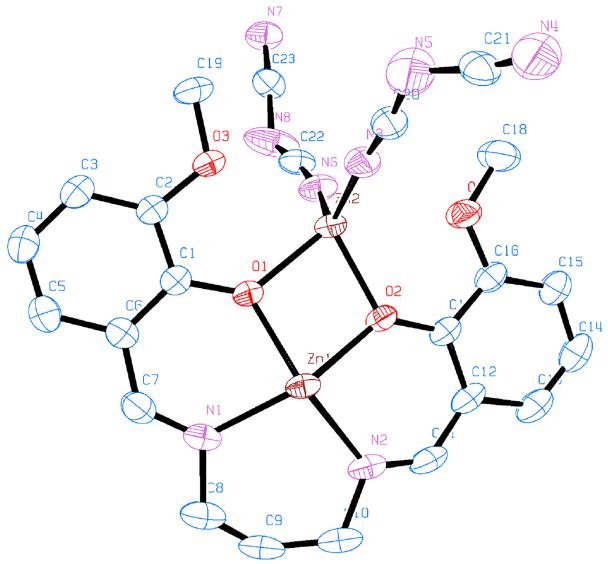

FIGURE 1 ORTEP diagram for CP1

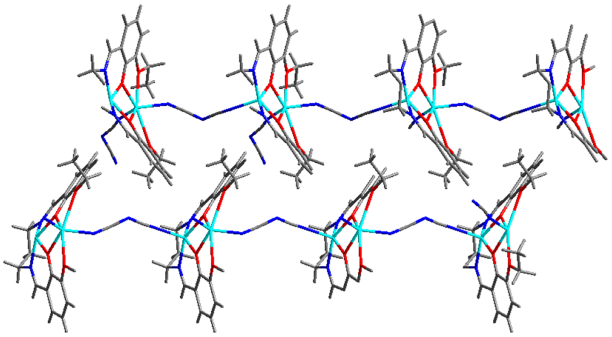

FIGURE 2 1-D Polymeric structure of **1**

contains two unsymmetrical tetradentate pockets [N2O2 and O4] which contains two Zn (II) metal ions. Apart from, this coordination action provided by the ligand $[L^{OMe}]^{2-}$, the di-nuclear zinc framework is further attached by dicyanamide ligand like a trunk of the insects (Figure 1). A close investigation into the crystal structure of CP**1** reveals that the asymmetric unit further grows by the dicyanamide ligand offers a one dimensional (1-D) polymeric chain (Figure 2). The two nearest 1D polymers further undergoes several non-covalent interactions (hydrogen bonding and C-H···π) and displays a two-dimensional polymeric framework (Figure S6). The coordination fashion of the ligands $[L^{OMe}]^{2-}$ and dicyanamide anions are shown in the Figure S6A which displays a fully deprotonated ligand coordinated with two Zn (II) ions in μ_2 – η1: η2: η1: η1: η2: η1 mode. The μ_2-phenolate oxygen atom acts as bridging ligand to construct Zn2(O)2 core whereas dicyanamide anion acts as a bridge between the two such di-nuclear core by using its $\mu_{1,5}$ coordination mode to afford a 1-D polymer (Figure 2). This type of dicyanamide bridging fashion is identical with previously reported bi-nuclear Schiff base complexes[82,83] and another dicyanamide ligand simply attached to the one of the zinc centers in the bimetallic core as a μ_1 mono dentate fashion. Two structurally independent Zn (II) centers are found in the single X-ray crystal structure. Zn(2) shows five coordination in a distorted square pyramidal geometry (Figure 3) which is composed by two imine nitrogen atoms and two phenolate oxygen atoms from deprotonated coordinating ligand, one N atom from dicyanamide anion where Addison parameter tau ()[82,83] value is 0.22 (= |β-α|/60^0) where β and α are the two largest angles around the central atom; = 0 for perfect square pyramidal and **1** for a perfect trigonal geometry). The calculated tau () value of CP**1** has been compared with literature reported Zn (II)-dicyanamide complexes (Table S6). On the other hand, Zn(1) is six coordinated satisfied from 4O, 2 N with a trigonal prismatic geometry (Figure 3). The bond lengths of zinc metal coordinated phenoxy atom are of range 2.011–2.043 Å while the metal coordinated nitrogen atoms are of range 2.045–2.063 Å. The bond angle Zn1-O2-Zn2 and Zn1-O1-Zn2 are 102.9° and 102.7° respectively. The distance between Zn(1) and Zn (2) metal centers is 3.165 Å which is comparable to other Zn—Zn separation of double phenoxo-bridged Zn_2 complexes.[11–14,84,85] All the bond angles and distances are comparable to those reported in the literature (Table S7).

4.2 | Crystal structure of CP2

Single crystal X-ray diffraction study of **2** reveals that this CP crystallizes in the orthorhombic space group, $P2_12_12_1$ (Z = 4) and asymmetric unit (Figure S7) contains two crystallographic independent zinc metal ions (Figure S7). The ORTEP diagram of asymmetric unit of CP**2** is given in the Figure 4. The structure is initially 1-D polymeric unit which undergoes several non-covalent interactions with the nearby another 1-D polymeric unit and ultimately furnish a 2-D layer (Figure S8) identical with

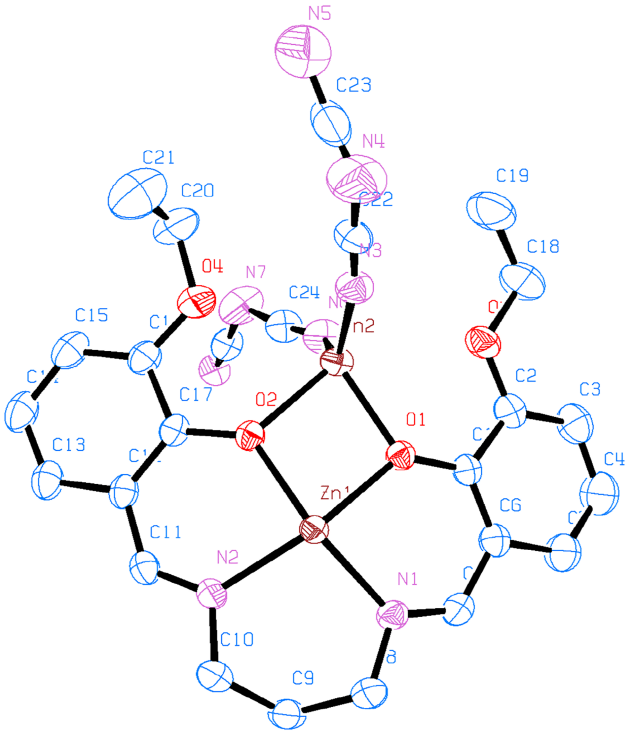

FIGURE 4 ORTEP diagram for CP**2**

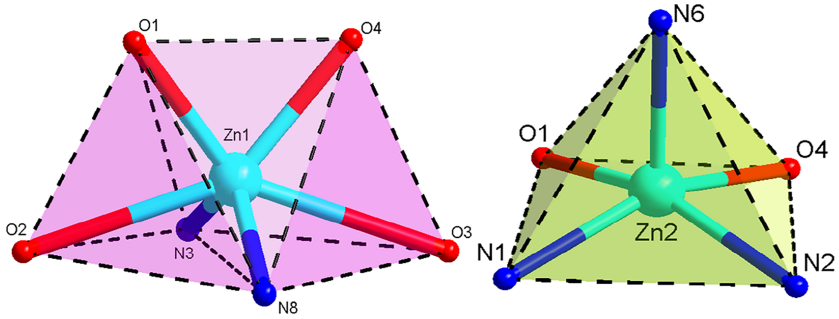

FIGURE 3 Zinc metal coordination environment in CP**1**

CP**1**. The binding mode of the main ligand, (H_2L^{OEt}) and co-ligand dicyanamide anion in the CP**2** is same as in **1** and the metal coordination environment (Figure S9 and Figure S10). Selected some important bond angle and bond lengths of CPs are given in the Table 4. Supplementary, the coordination motifs of present investigated ligands have been compared with identical compartmental ligands in terms of ligand anionic donor centers, CPs formation, dicyanamide spacer bridging flexibility (Table S8).

4.3 | Hirshfeld surface

HS analysis is generally used to study the intermolecular forces between different molecules and intra molecular interaction within a molecule in a crystal lattice. Molecular electrostatic potential mapping on the HS acts as a tool to study electrostatic complementarily between nearby molecules, which provides basic knowledge about the crystal packing. Total electrostatic interactions are determined as a sum of electrostatic interaction, polarization, dispersion and exchange repulsion which all are calibrated against dispersion corrected DFT.[86–88] For CP**1**, the D_{norm}, shape Index, fragment patch and curved Index are provided in Figure 5. The total volume of the surface is 623.69 A^3, globularity is 0.682 and asphericity 0.030. This shows that the CP**1** deviates from perfect spherical shape whereas for CP**2**, globularity value is 0.695 and asphericity value is 0.02. These values suggest that CP**1** is more deviate from the sphericity than CP**2** (Figure 6). 2-D fingerprint plots (Figure 5 and Figure 6) provides information about different types of possible interactions between CPs and other atoms of the surround molecules (Table S9). For CP**1**, the highest interaction is between hydrogen atoms and there is no interaction between O atoms and Zn atoms, due to their high electronegativity and electro positivity. For CP**2**, the results are slightly different from that of CP**1** where no interaction observed between O atoms, Zn atoms and N atoms. The highest interaction is between the hydrogen atoms and also between C and H followed by N and H.

TABLE 4 Selected important bond distances (Å) and angles (°) for CP**1** and CP**2**

Bond lengths (Å)	Value (Å)	Bond angles (°)	Value (°)
1			
Zn1-N1	2.063(5)	N1-Zn1-N2	96.5(2)
Zn1-N2	2.045(4)	O1-Zn1-O2	75.4(1)
Zn1-N6	1.943(6)	N8-Zn1-N2	106.0(2)
Zn1-O1	2.043(2)	N8-Zn1-N1	100.5(2)
Zn1-O2	2.040(3)	O1-Zn1-N1	88.0(1)
Zn1-N8	2.025(4)	O2-Zn1-N2	89.3(1)
Zn2-O2	2.006(3)	O1-Zn2-O2	75.4(1)
Zn2-O1	2.011(3)	N3-Zn2-N6	119.3(2)
Zn2-O4	2.540(4)	N3-Zn2-O4	80.9(1)
Zn2-N6	1.973(4)	N6-Zn2-O1	109.1(1)
Zn2-N3	1.949(5)	N6-Zn2-O2	113.5(1)
2			
Zn1-O1	2.012(2)	O1-Zn1-O4	146.5(1)
Zn1-O2	2.574(3)	N3-Zn1-N8	124.8(2)
Zn1-O4	2.001(3)	O2-Zn1-O4	146.5(1)
Zn1-N8	1.980(4)	O1-Zn1-O2	67.8(1)
Zn1-N3	1.938(4)	O1-Zn2-O4	76.6(1)
Zn2-N2	2.048(3)	N1-Zn2-N2	94.7(1)
Zn2-N1	2.058(3)	O1-Zn2-N6	100.6(1)
Zn2-N6	2.018(4)	N1-Zn2-N6	105.3(1)
Zn2-O1	2.026(3)	N2-Zn2-N6	104.8(1)
Zn2-O4	2.079(3)	-	-

4.4 | FMO

Frontier molecular orbital (FMO) provides useful information about the reactivity and stability of dicyanamide modulated zinc metal CPs. Visualizations of the HOMO and LUMO can provide some interesting insights about the nature of the CPs and its reactivity and other physicochemical characteristics. Figure S11-12 provides the pictorial representations of the frontier molecular orbitals of the CP**1** and CP**2**. It shows that for both CPs, HOMO is predominantly placed over the Zn atoms and LUMO is delocalized over the aromatic *ortho* vanillin condensed Schiff base ligands coordinated to the central metal atoms. The energy values obtained from FMO's can be used to generate other different reactivity parameters. These data can be used to find other frontier orbital data as follows, ionization potential: $I = -E_{HOMO}$, electron affinity $A = -E_{LUMO}$, hardness $\eta = (I-A)/2$, and electrophilicity index $\omega = \mu^2/2\eta$.[89] For CP**1**, energy of HOMO and LUMO are −8.7827 and − 2.9777 eV respectively, the vertical excitation energy gap, which is the difference between HOMO and LUMO is 2.8050 eV. The ionization energy is 5.7827 and electron affinity A, 2.977, global electronegativity 4.3802, hardness 1.4025, chemical potential −4.3802, electrophilicity index 6.8402 and global softness 0.7130 (eV). Data for CP**2** is only slightly different where HOMO is at −5.8110 eV, LUMO at −2.9315, energy gap 2.8795, ionization energy 5.110, electron

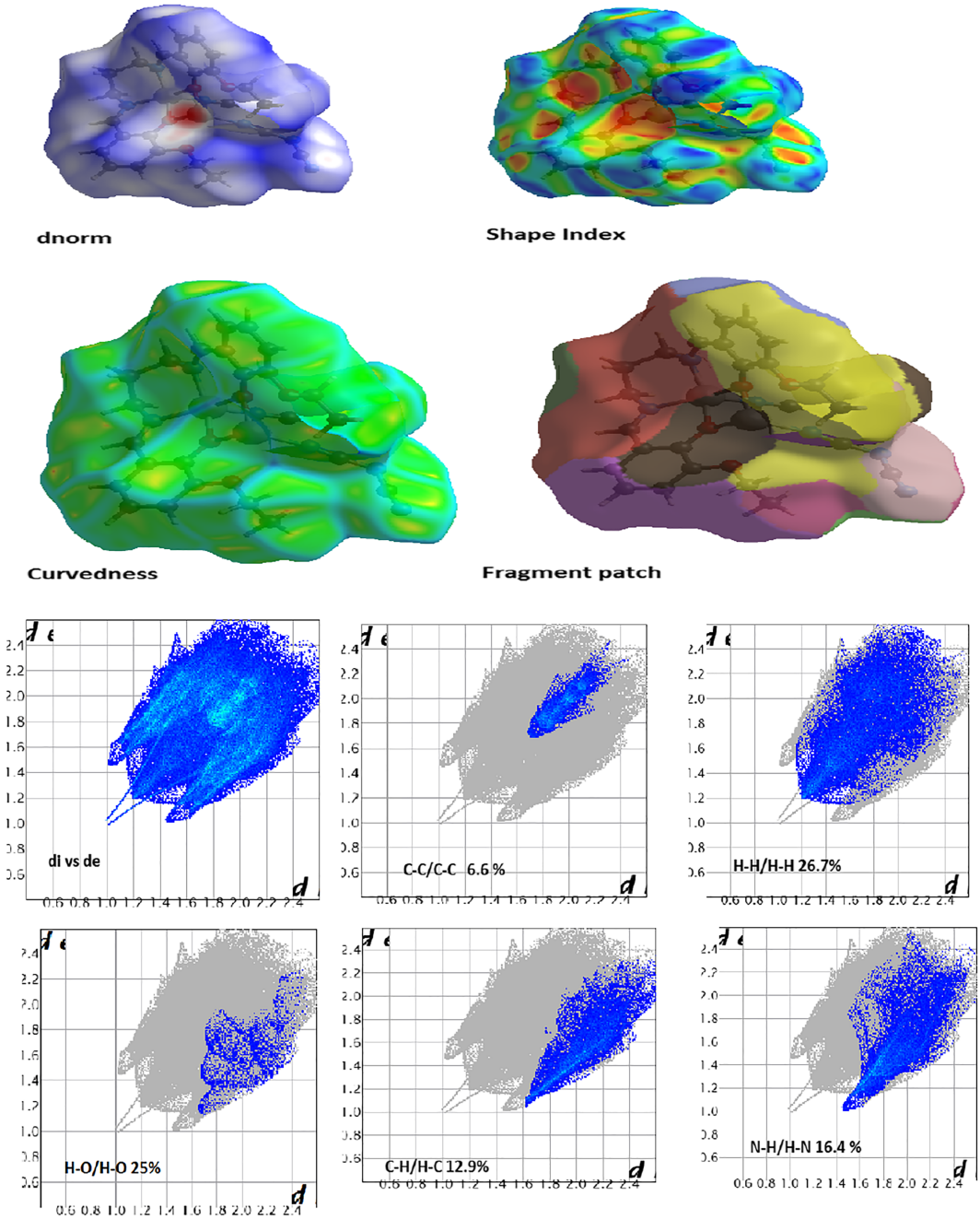

FIGURE 5 Hirshfeld surface analysis for CP**1**: d_{norm}, Shape index, curvedness and different 2D fingerprint plots

affinity 2.9315, electronegativity 4.3712, global hardness 1.4398, chemical potential −4.3712, electrophilicity index 6.6358 and global softness 0.6946 (all values in eV). High energy gap, ionization energy, lower electron affinity, electronegativity, high hardness, low electrophilicity index and softness are for CP**2**, which means that CP**2** is more stable than CP**1**. Partial density of states (PDOS) of CPs are provided in Figure S13-14 which indicates that there is not much orbital overlap in the core molecular orbitals.

4.5 | TD-DFT

The simulated UV–Vis spectral data can be used to determine whether the CPs utilized in a Dye Sensitized Solar Cell (DSSC) as a potential photosensitizer, which absorbs energy from light and undergoes electronic transition and later transferred the gained energy to the TiO2 semiconductor, which completes the electronic circuit in the solar cell. The ability of the CPs, called the light harvesting efficiency (LHE) to absorb the light depends on its oscillator

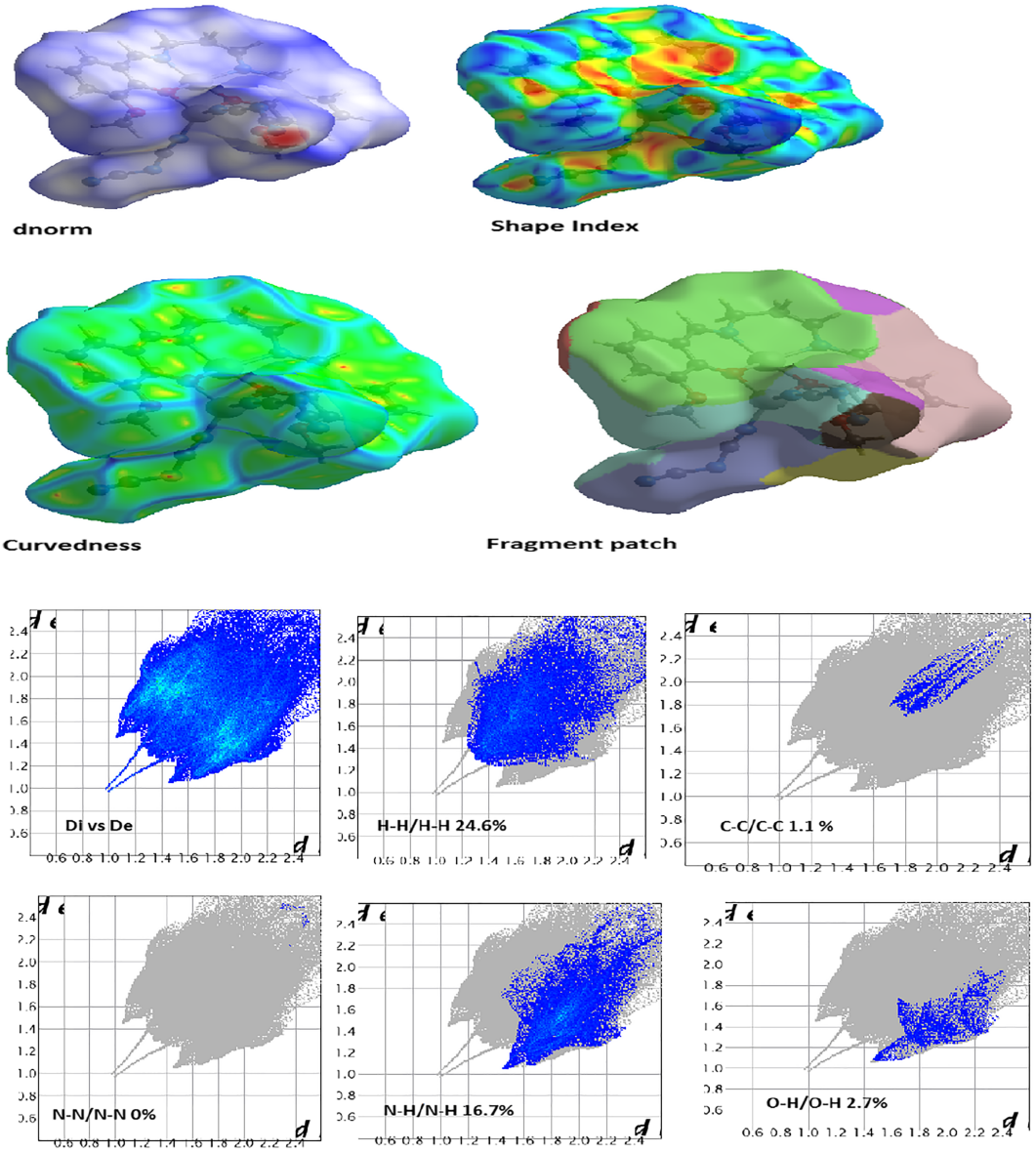

FIGURE 6 Hirshfeld surface analysis for CP**2**: d_{norm}, Shape index, curvedness and different 2D fingerprint plots

strength (f) by the relation following (LHE) = $1\text{-}10^{-f}.\Phi_{inject}$ or the electron injection efficacy is a very important parameter that decides the efficiency of the DSSC. It is almost synonymous to the driving force ΔG_{inject}. The electrons injecting from the excited states of CPs to the semiconductor is obtained from the difference between the excited state oxidation potential (E^*_{Oxi}) and E_{CB} is the ground state reduction potential of TiO_2 conduction band ($E_{CB} = -4.0$ eV). ΔG_{inject} is calculated by using the popular equation, $\Delta G_{inject} = E^*_{Oxi} - E_{CB}$ where E^*_{Oxi} is calculated from the ground state redox potential of sensitizers (E_{Oxi}) and vertical transition energy corresponding to the maximum absorption (E_{00}) can be written as: $E^*_{Oxi} = E_{Oxi} - E_{00}$. For CP**1**, two major electronic transitions are observed at wavelength 325.79 nm and 267.26 nm with oscillating strengths 0.38 and 0.6396 respectively. The experimental values are 358 nm and 276 nm. The first transition is due to HOMO-1 to LUMO (43%) and HOMO to LUMO+1 (51%), while the second transition is contributed by HOMO-5 to LUMO +1 (29%), HOMO-4 to LUMO (39%) and HOMO-3 to LUMO (13%) (Table S10A†). Both transitions are from singlet ground state HOMO orbitals to the excited state orbital of A symmetry. In case of CP**2**, there are again two absorption wavelengths at 327.88 nm and 268.68 nm with an oscillator strength of 0.3732 and 0.6237 respectively. The experimental UV–Vis values are at 356 nm and 275 nm. Symmetrically, they are from the singlet state to the states of A symmetry. The transition at 327.88 nm is contributed by HOMO-1 to LUMO (44%) and HOMO

to LUMO+1 (51%) and for the transition at 268.68 is contributed by HOMO-5 to LUMO +1 (29%), HOMO-4 to LUMO (25%) and HOMO-3 to LUMO (20%) (Table S10B). The light harvesting efficiency (LHE) for transition 1 is 0.5861 and for the second is 0.7707, which means that during the second transition 77.07% of the incident solar energy is absorbed by the CP**1**. ΔG_{inject} values are calculated and provided in the Table S11. For CP**1**, the values are −2.0234 ev and − 2.8569 eV. The data clearly indicates that the second transition is more feasible than the other with more negative Gibb's free energy values. For CP**2**, the free energy of injection values are −1.9709 eV and − 2.4262 eV which is less than CP**1**. Generally, free energy values can predict the spontaneity of a process. More negative the free energy, more spontaneous or feasible the process is. Therefore, finally it can be concluded that CP**1** is having more use in DSSC's than CP**2**.

5 | PHOTOLUMINESCENCE

Photoluminescence properties of Schiff base ligands and CPs are monitored in spectroscopic grade DMSO solvent (Table 5). In DMSO, the fluorescence emission spectra (Figure 7) revealing that free ligands are practically weak fluorescence with respect to CPs. Upon photo excitation at 332 nm, 338 nm, Schiff base ligands exhibit fluorescent emission maxima centered at 390 nm and 423 nm. Similarly, CPs upon photo excitation at wavelength 359 nm, 356 nm shows fluorescence maxima with the major emission peak at 470 nm and 475 nm. The increased fluorescence emission intensity of CPs over free ligands may probably due to N, O-donor centers effective coordination with the Zn (II) metal ion, thereby increasing the conformational rigidity via chelation effect [CHEF] and subsequently loss of energy by radiation less thermal vibration. Besides, the active fluorescence nature of CPs compared to free ligands may be due to d^{10} configuration zinc metal ion is difficult or hard to oxidize or reduce. This type of fluorescence nature may be assigned due to the intra-ligand ($\pi \rightarrow \pi^*$) transition or L → M charge transfer popularly referred as CHEF (Chelation enhanced fluorescence)[90–98] whereas for quenching "Chelation

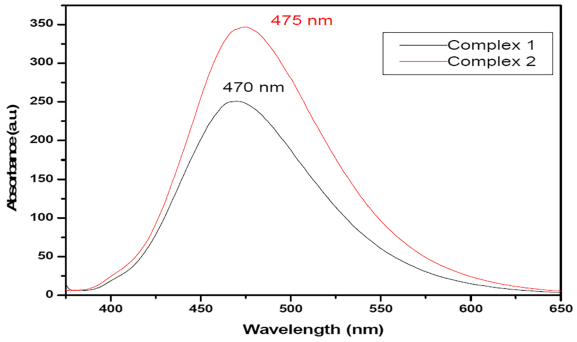

FIGURE 7 Ligand-centered Fluorescence emission spectra for CP**1** and CP**2**

enhancement of Quenching effect" (CHEQ) is recommended.[99] The nature of emission spectra of ligands and CPs are comparable with previously reported salen-type ligands[73,84,85] as well as Zn (II)-dicyanamide complexes (Table S12). The low quantum yield of Schiff base ligands is ascribed due to fast Photoinduced electron transfer (PET) from nitrogen lone pair to the conjugated phenolic moiety. L-M complexation prevents PET process thereby enhances quantum yield (ϕ) in the CPs.[100–102] Since ligands exhibit chrematistic fluorescence emission, hence solid-state fluorescence spectroscopic studies have been undertaken mainly for CPs.[103] Under solid-state, photo excitation at similar wavelength shows photoluminescence with the main emission intense peak near at 464 nm and 462 nm (Figure 8). This type of electronic transitions is assigned due to intra-ligand ($\pi \rightarrow \pi^*$)

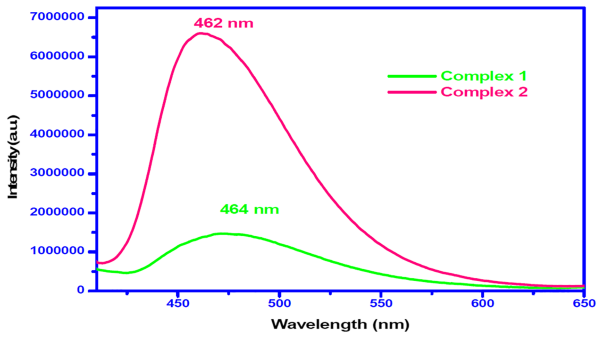

FIGURE 8 Solid-state Fluorescence emission spectra for CP**1** and CP**2**

TABLE 5 Summary of steady state and time-resolved photoluminescence decay

Compounds	λ_{ex} (nm)	λ_{em} (nm)	λ_{em} (nm) [Solid-state]	Quantum Yield (ϕ)	τ_1[ns]	τ_2[ns]	$<\tau>$ [ns]	χ^2
CP**1**	359	470	464	0.01211	0.76 (99%)	7.87% (1%)	1.11	1.27
CP**2**	356	475	462	0.01453	0.63 (99%)	7.92 (1%)	1.06	1.26
(H_2L^{OMe})	332	390	-	0.00352				
(H_2L^{OEt})	338	423	-	0.00359				

transitions. Therefore, CPs fluorescence nature are more active in solution than solid-state. Interestingly, the fluorescence emission maxima of CPs are more bathochromically red shifted in DMSO solvent than solid-state environment. Therefore, in DMSO, the fluorescence behaviours of CPs are mainly ligand centred whereas in solid-state it is totally crystal packing dependent.[103] To get a better understanding on emitting properties of CPs, time-resolved fluorescence spectroscopic studies have been measured in DMSO (Figure S15). The fluorescence lifetime for CPs have been measured upon excitation at 359 nm and 356 nm. The nature of decay profile will be best fitted to bi-exponential nature (with acceptable comparable χ^2 values) which are comparable with reported Zn (II)-salen-type complexes.[73,103–108] In DMSO, a regular trend observed for fluorescence lifetimes where CPs shows two different decay times having maximum (99%) and minimum (1%) contribution in amplitude. The fluorescence lifetime value further divulges that importance of excited states stabilities of CP**1** are greater than CP**2**. The bi-exponential decay profiles for CPs are best explained as due to competition of different excited states that is $\pi \rightarrow \pi^*$ excited states involved in the emission features and preferably CT character that quenches the fluorescence.[104,105]

6 | THERMAL ANALYSIS

Thermal characteristics of the CPs were studied using TG-DTG techniques under nitrogen atmosphere. In the CP**1**, a mass loss of about of about 11.34% (calculated 11.98%, Figure S16[a]) in the temperature range 207–349.77 °C which corresponds to the loss of the $\mu_{1,5}$-dicyanamide linker units. A second mass loss of about 20.1% (calculated 21.5%) is observed in the range 440–652°C which corresponds to the loss of the methoxy units in the CP. On further heating up to 1000 °C the CP continues to disintegrate. The thermal behavior of CP**2** is different when compared to that of **1**. In **2**, a continues of decomposition of the CP can be seen in the broad temperature range from 211 to 685 °C which includes the disintegration of the $\mu_{1,5}$-dicyanamide linker units, diimine spacer unit and ethoxy units from the CP and the which has a total mass loss of about 60.07% (calculated 59.21%, Figure S16[b]). On further heating the CP continues to decompose. It can be seen that the thermal stability of CP**1** is relatively high when compared to that of **2** where the later exhibits dismal thermal stability where there is continues decomposition starting from ca. 200 °C.

7 | CYTOTOXICITY ANALYSIS

We screened synthesized ligands S1B (H_2L^{OMe})/S2C (H_2L^{OEt}) and their corresponding dicyanamide modulated zinc metal CPs, S2A for CP**1** and S2D for CP**2** respectively against three cancerous cell lines using MTT assay viz., MCF7 (breast cancer), MDA-MB-231 (breast carcinoma) and MCF10A (breast epithelial) to determine their toxicity and inhibitory concentrations (IC_{50}). Based on the analysis of cytotoxic activity of four synthesized compounds, CP**1** to be most potent against MCF7 and MDA-MB-231 cancerous cell lines. The CP**1** exhibited the IC_{50} value at 20 μM for (MCF7) and 15 for (MDA-MB-231) whereas the other showed a high IC_{50}

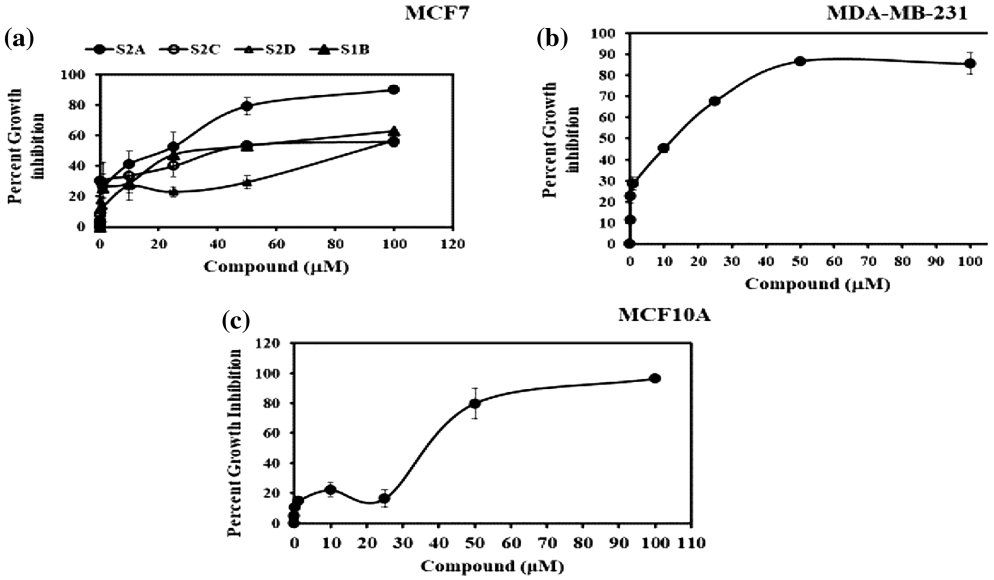

FIGURE 9 **A–C** Cytotoxic effect against breast cancer cell lines of ligands and CP**1**-CP**2**

value with (H_2L^{OMe}) at 50 μM (MCF7), (H_2L^{OEt}) at 47 μM (MCF7) and CP**2** at 60 μM concentrations (MCF7) (Figure 9(A)). Further, four screened compounds IC_{50} values have been compared with previously reported Zn (II)-Schiff base complexes as well as anticancer drug cisplatin (Table 6).[109–116] Among the four compounds, only CP**1** was found to be good cytotoxicity with MCF7 cell line. We then further proceed with CP**1** and performed a similar screen in MDA-MB-231 cell line. The results revealed an even lower IC_{50} value (15 μM) of CP**1** in this cell line (Figure 9(B)-9(C)). Therefore, in between MCF7 and MDA-MB-231 cell lines, CP**1** is active only with MDA-MB-231 over CP2 or free Schiff base ligands. Further, since two Schiff bases are identical structure except intervened -CH_2-moiety with respect to OH group at ortho position, their cytotoxic variation in MCF7 and MDA-MB-231 cell lines are significantly small.[110] The cytotoxic behavior of zinc metal CPs is preferentially dependent on their ability to bind with DNA. The potency of cytotoxic effect may also be attributed with positive charge of the metal atom (here Zn^{2+}ion) which increased the acidity of proton of coordinated ligands and causes stronger hydrogen bonding, thereby enhancing biological activity. Generally, damage of DNA structure results in the impairment of its function, which eventually causes cell death. A clear variation of cytotoxicity was observed particularly in presence of variable coordinated substituents and different nature of metal ions (our synthesized CPs possess common Zn^{2+} ion). This is basically due to the alternation in binding ability of DNA.[117,118] Synthesized both CPs are dicyanamide bridged 1-D chain polymer, therefore CP**1** cytotoxic variation against MCF7 and MDA-MB-231 cell lines are nearly identical. Further, it was construed that in CP**2** greater electron releasing substituents effect of Schiff base ligand (H_2L^{OEt}) significantly enhances cytotoxicity against MCF7 breast cancer cell line.[110] This difference may be attributed due to the introduction of -OEt with

TABLE 6 IC_{50} values for CP**1**-CP**2** and previously reported Zn (II)/cisplatin complexes against breast cancer cell lines (MCF7, MDA-MB-231, MCF10A) using MTT assay

Compounds	IC_{50} values (μM)			Ref
	MCF7	MDA-MB-231	MCF10A	
CP**1**	20	15	40	This work
CP**2**	60	-	-	This work
(H_2L^{OMe})	50	-	-	This work
(H_2L^{OEt})	47	-	-	This work
[$Zn_4(L^{OMe})_2(\mu_1\text{-dca})_2$ ($\mu_{1,5}$-dca)] [$Zn_3(L^{OEt})_2$ (H_2O)(μ_1-dca)($\mu_{1,5}$-dca)]	46.6 ± 10.69 47.8 ± 10.78	-	-	57
[$Zn(L_2)(OAC)_2.2H_2O$]	16.8 ± 0.21	-	-	109
[$Zn(L_1).2H_2O$]	6.7 ± 0.18	-	-	110
[$Zn(L_2).2H_2O$]	4.3 ± 0.31			
[$Zn(L_3).2H_2O$]	58.9 ± 0.62			
[$ZnL^1(OAc)_2$]PF_6	16.21	-	-	111
[$ZnL^1(OAc)_2$](BPh_4	14.72			
[$Zn(L^2)_2$]	-	2.0	-	112
[$Zn(L^3)_2$]				
[Zn(L)]	14.9–22.2	-	-	113
[$Zn(L)_2$]	26 ± 1.8	-	-	114
[Zn $(Br)_2L^1$]	1.05			115
[Zn $(Br)_2L^2$]	1.064			
[Zn $(Br)_2L^3$]	2.319			
[$Zn(I)_2L^1$]	0.899			
[$Zn(I)_2L^2$]	1.265			
[$Zn(I)_2L^3$]	3.049			
Cisplatin	42.2 ± 8	128.2 ± 7	-	116

respect to hydroxyl group in o-vanillin. Finally, the overall discussion implies that the electronic effect may be one of the influential factors in determining the anticancer activities of dicyanamide modulated Zn (II)-CPs.

7.1 | Colony formation assay

To further identify its effect on the non-cancerous normal breast epithelial cells, we screened CP**1** in MCF10A cell lines and observed a high IC_{50} value (40 μM) denoting the lesser toxicity of CP**1** on the normal cells. The low IC_{50} values obtained for CP**1** in both MCF7 and MDA-MB-231 cell lines prompted us to check the effect of this CP on the long-term growth of these cells. We, therefore, performed the colony formation assay in both the cell lines. We found that treatment of cells with their effective IC_{50} concentrations led to a reduction in the number as well as the size of colonies formed (Figure 10).

7.2 | Apoptosis/autophagy/necrosis

Apoptosis, autophagy and necrosis are recognized as the classical cell death pathways which involve different mechanisms and morphological features.[119,120] The smaller and lesser number of colonies observed in the presence of CP**1** led us to check if the complex induced any form of cell death. We treated MDA-MB-231 cells with two different concentrations of CP**1** and checked the expression levels of proteins involved in apoptosis. We observed a decrease in the pro-apoptotic protein levels PUMA and BAX and lack of cleaved caspase-8 and caspase-9 in presence of CP**1** (Figure 11(A)) indicating that CP**1** does not inhibit the growth of cancer cells through induction of apoptosis. Furthermore, the 89 kDa cleaved product of PARP was not seen in the nuclear cytoplasmic fractionation (Figure 11(B)) ascertaining the earlier observation. To corroborate the finding, we performed the DNA fragmentation assay and did not observe the ladder of fragmented DNA in the cells treated with CP**1** (Figure 11 (C)). All these data depict that CP**1** does not induce apoptosis. To decipher the cause of reduction in cell number in presence of CP**1**, we checked for the other mode of cell death. To this end, we checked for necrosis by observing the pattern of PARP cleavage but did not find a 55 kDa cleavage product which is a marker of necrosis. We further checked for the possibility of autophagic cell death induction by the CP**1**. Though we have detected a reduction in p-mTOR and pS6K levels (Figure 12(A)), which is a characteristic of autophagy initiation. The autophagy driven cell death is associated with increased levels of Beclin as well as LC3BII and decreased levels of p62. However, we obtained contrasting results wherein the expression levels of Beclin and LC3BII were decreased and the levels of p62 were increased (Figure 12(B)) denoting the absence of autophagy-induced cell death. Cumulatively, these observations infer that CP**1** may utilize some other non-classical death mechanism to limit the number of breast cancer cells. Maintenance of normal cell cycle is essential for the cellular growth and proliferation. Since CP**1**

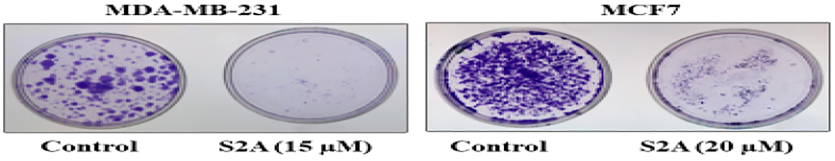

FIGURE 10 Colony formation assay of CP**1**

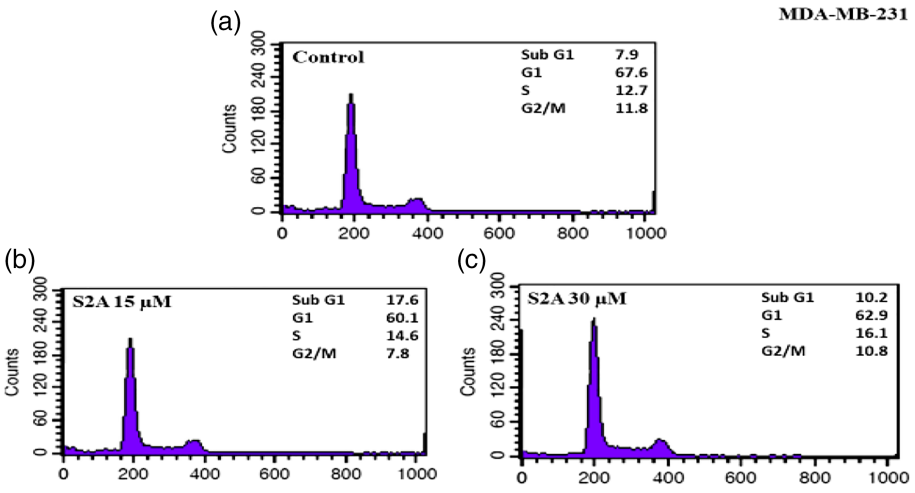

FIGURE 11 A–C Effect of CP**1** against MDA-MB-231 cells

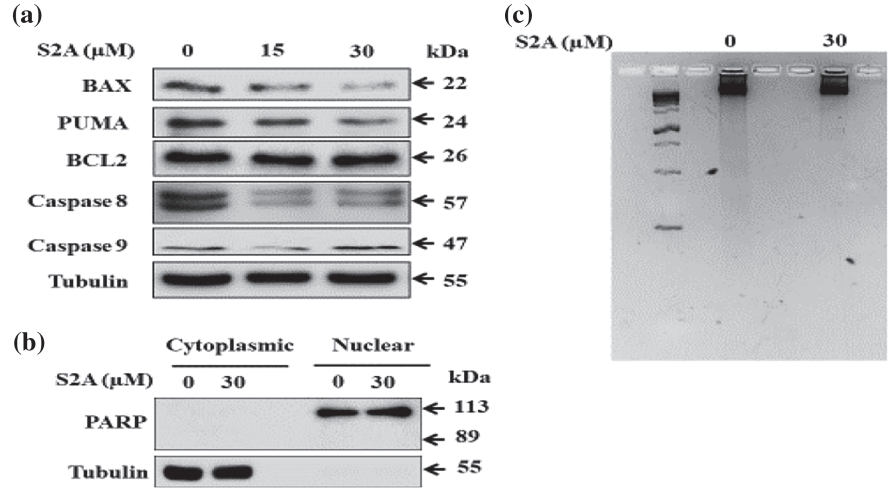

FIGURE 12 A–B The autophagic cell death induction by CP**1**

inhibits the cell proliferation, we went ahead to check if **1** interferes with the normal functioning of the cell cycle thereby inhibiting the cellular growth. The cell cycle profile was examined through FACS analysis. Results demonstrated a normal cell cycle profile with no apparent differences observed in any phases of the cell cycle showing that **1** does not control the cell cycle (Figure 13). In addition to the cell cycle, cell proliferation is largely controlled by the multitudes of signaling pathways functioning in the cells. Since, we found that CP**1** does not alter the cell cycle, we went ahead to decipher its effect on major proliferative pathways of the cell in the MDA-MB-231 cells. We observed a decrease in the levels of phospho- and total levels of MEK and ERK with concomitant increase in the dose of CP**1** (Figure 14). Furthermore, a similar observation was made for PI3K/AKT pathway as well. The phospho-AKT473 and the total AKT levels were found to decrease in MDA-MB-231 cells (Figure 14).

These observations indicate towards the negative regulation of two major cell proliferation pathways by CP**1**. The inhibition of MAPK and PI3K/AKT pathways may play a partial role for the observed reduction in growth of cells. To further discern the effect of CP**1** on normal breast epithelial cells, we treated both the non-malignant breast cells MCF10A and the malignant cells MDA-MB-231 with the IC_{50} dose of CP**1** for MDA-MB-231 cells.

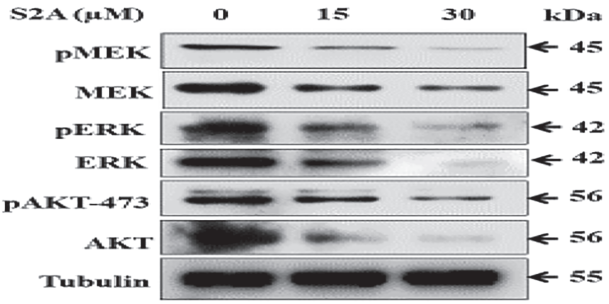

FIGURE 14 Major proliferative pathways of MDA-MB-231 cells of CP**1**

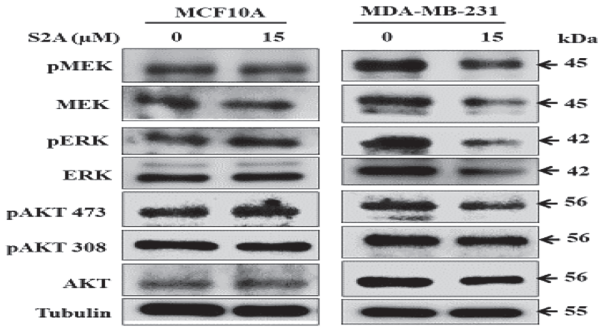

FIGURE 15 Major proliferative pathways of MDA-MB-231 cells of CP**1**

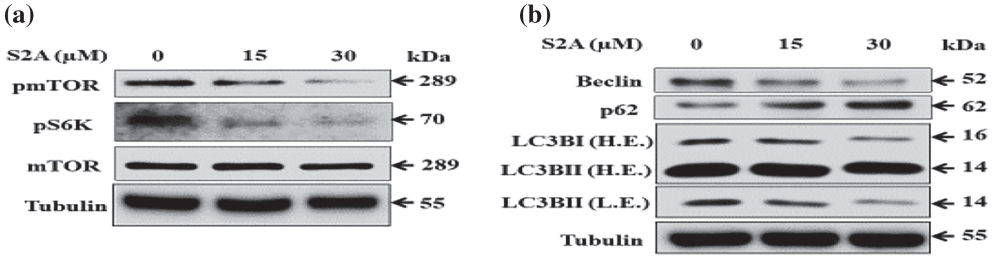

FIGURE 13 FACS analysis of CP**1**

We observed the expected reduction in expression levels of MAPK/ERK pathway and the PI3K/AKT pathway in MDA-MB-231 cells but did not detect any difference in the MCF10A cells (Figure 15) indicating the utility of CP**1** in cancer therapeutics.

8 | CONCLUSIONS

This research article describes the syntheses and structural aspects of the dicyanamide-bridged 1-D chain zinc metal coordination polymers (**1**–**2**). The successful syntheses of CPs were only achieved in presence of *ortho* vanillin derived Schiff base ligands after utilizing properly their compartmental $N_2O_2^-$ and O_4^- donor sets. Solid-state X-ray single crystal study revealed two different geometrical environment of Zn metal centers with distorted square pyramidal Zn(2) and trigonal prismatic Zn(1) geometry. DFT using B3LYP and DGDVP basis sets were successfully applied to explain FMO, HS, TD-DFT and photovoltaic efficiency in Dye Sensitized Solar Cell (DSSC). The Steady state and time-resolved fluorescence measurements were conducted in DMSO and solid-state condition at room temperature. The thermal stabilities of CPs have been examined by TGA. CPs as well as Schiff base ligands evinced potential cytotoxic effects on breast cancer cells using MTT assay, MCF7, MDA-MB-231 and MCF10A. In vitro cytotoxicity assessment confirmed CP**1** to be most potent against MDA-MB-231 cell line and even anticancer drug cisplatin. Supplementary, programmed cell death apoptosis, autophagy and necrosis were successfully highlighted in this research article. To the best of our knowledge dicyanamide-bridged Zn (II)-CPs photovoltaic efficiency in Dye Sensitized Solar Cell and cancerous activities are seems to be rare in literature. Thus, the prospective study in the present manuscript deals a new insight of CP**1** in the development of cancer therapeutics.

9 | APPENDIX A. SUPPLEMENTARY MATERIAL

Details supplementary data related to this article can be associated in ESM_AOC. CCDC number 1901797–1901798 contains the supplementary crystallographic data (excluding structure factors) in CIF format for the structure reported of complexes. Copies of the data can be obtained, free of charge, on application to CCDC, 12 Union Road, Cambridge CB2 1EZ, U.K.: http://www.ccdc.cam.ac.uk/cgi-bin/catreq.cgi, e-mail: data_request@ccdc.cam.ac.uk, or.

ACKNOWLEDGMENTS

This research work did not receive any specific grant from funding agencies in the public, commercial or not-profit sectors. Dr. Dipankar Mishra gratefully acknowledges the financial grant sanctioned by UGC, New Delhi, in his favor vide Minor Research Project (F.PSW-232/15-16(ERO). D. J. Majumdar thanks Mr. Surajit Mondal, Research Scholar, IIT-ISM, Dhanbad-826004, India for ^{1}H NMR spectroscopic help and Dr. S. S. Sreejith, Cochin University of Science and Technology, Kochi-682022, Kerala, India for Thermogravimetric analysis help.

CONFLICT OF INTEREST

Author declare no potential conflict of interest.

ORCID

Dhrubajyoti Majumdar https://orcid.org/0000-0002-9785-7750
Sourav Das https://orcid.org/0000-0002-3346-5598
Dipankar Mishra https://orcid.org/0000-0002-0216-8400

REFERENCES

[1] X. Q. Zhang, Y. F. Gao, H. T. Liu, Z. L. Liu, *CrystEngComm* **2015**, *17*, 6037.

[2] J. He, M. Zeller, A. D. Hunter, Z. Xu, *CrystEngComm* **2015**, *17*, 9254.

[3] H. L. Nguyen, F. Gandara, H. Furukawa, T. L. Doan, K. E. Cordova, O. M. Yaghi, *J. Am. Chem. Soc.* **2016**, *138*, 4330.

[4] X. S. Wu, J. Liang, X. L. Hu, X. L. Wang, B. Q. Song, Y. Q. Jiao, Z. M. Su, *Cryst. Growth des.* **2015**, *15*, 4311.

[5] B. Mohapatra, S. Verma, *Cryst. Growth des.* **2016**, *16*, 696.

[6] C. Wang, F. Xing, Y. L. Bai, Y. Zhao, M. X. Li, S. Zhu, *Cryst. Growth des.* **2016**, *16*, 2277.

[7] X. C. Shan, F. L. Jiang, D. Q. Yuan, M. Y. Wu, S. Q. Zhang, M. C. Hong, *Dalton Trans* **2012**, *41*, 9411.

[8] A. B. Nowakowski, J. W. Meeusen, H. Menden, H. Tomasiewicz, *Inorg. Chem.* **2015**, *54*, 11637.

[9] F. Jones, *CrystEngComm* **2012**, *14*, 8374.

[10] L. Guang, J. T. Hupp, *J. Am. Chem. Soc.* **2010**, *132*, 7832.

[11] D. J. Majumdar, S. Dey, S. S. Sreekumar, S. Das, D. Das, J. K. Biswas, M. Mondal, P. Shukla, T. Pal, K. Bankura, D. Mishra, *J. Mol. Struct.* **2019**, *1179*, 694.

[12] D. J. Majumdar, D. Das, S. S. Sreejith, S. Das, J. K. Biswas, M. Mondal, D. Ghosh, K. Bankura, D. Mishra, *Inorg. Chim. Acta* **2019**, *489*, 244.

[13] D. J. Majumdar, M. S. Surendra Babu, S. Das, J. K. Biswas, M. Mondal, *J. Mol. Struct.* **2017**, *1138*, 161.

[14] D. J. Majumdar, M. S. Surendra Babu, S. Das, C. Mohapatra, J. K. Biswas, M. Mondal, *ChemistrySelect* **2017**, *2*, 4811.

[15] B. Naskar, R. Modak, D. K. Maiti, M. G. B. Drew, A. Bauza, A. Frontera, C. D. Mukhopadhyay, S. Mishra, K. D. Saha, S. Goswami, *Dalton Trans* **2017**, *46*, 9498.

[16] V. Liuzzo, W. Oberhauser, A. Pucci, *Inorg. Chem. Commun.* **2013**, *13*, 686.

[17] A. Tsaturyan, Y. Mchida, T. Akitsu, I. Gozhikova, I. Shcherbacov, *J. Mol. Struct.* **2018**, *1162*, 54.

[18] E. Guzel, *RSC Adv.* **2019**, *9*, 10854.

[19] Y. -W. Dong, R. -Q. Fan, P. Wang, L. -G. Wei, X. -M. Wang, H. -J. Zhang, S. Gao, Y. L. Yang, Y. -L. Wang, *Dalton Trans* **2015**, *44*, 5306.

[20] M. Andruh, *Chem Commun* **2011**, *47*, 3025.

[21] M. Andruh, *Dalton Trans* **2015**, *44*, 16633.

[22] J. Long, F. Habib, P. H. Lin, I. Korobkov, G. Enright, L. Ungur, W. Wernsdorfer, L. F. Chibotaru, M. Murugesu, *J. Am. Chem. Soc.* **2011**, *133*, 5319.

[23] E. C. Webb, *Enzyme Nomenclature: Recommendations of the Nomenclature Committee of the International Union of Biochemistry and Molecular Biology*, Academic Press, New York **1992**.

[24] J. Emsley, *Nature's Building Blocks: An A–Z Guide to the Elements*, Oxford University Press, Oxford **2011**.

[25] A. I. Bush, *Trends Neuro Sci* **2003**, *26*, 207.

[26] D. Noy, I. Solomonov, O. Sinkevich, T. Arad, K. Kjaer, I. Sagi, *J. Am. Chem. Soc.* **2008**, *130*, 1376.

[27] W. N. Lipscomb, N. Strater, *Chem. Rev.* **1996**, *96*, 2375.

[28] I. Bertini, H. B. Gray, S. J. Lippard, J. S. Valentine, *Bioinorganic Chemistry*, University Science Books, Mill Valley, CA **1994**.

[29] M. T. Tarafder, K. T. Jin, K. A. Crouse, A. Ali, B. Yamin, H. -K. Fun, *Polyhedron* **2002**, *21*, 2547.

[30] A. Alsalme, S. Laeeq, S. Dwivedi, M. S. Khan, K. Al Farhan, J. Musarrat, R. A. Khan, *Spectrochimica Acta - Part a: Molecular and Biomolecular Spectroscopy* **2016**, *163*, 1.

[31] H. M. Aly, M. E. Moustafa, M. Y. Nassar, E. A. Abdelrahman, *J. Mol. Struct.* **2015**, *1086*, 23.

[32] Z. L. He, X. E. Yang, P. J. Stoffella, *J. Trace Elem. Med. Biol.* **2005**, *19*, 125.

[33] M. Hamatake, K. Iguchi, K. Hirano, R. Ishida, *J. Biochem.* **2000**, *128*, 933.

[34] D. Magda, P. Lecane, Z. Wang, W. Hu, P. Thiemann, X. Ma, *Cancer Res.* **2008**, *68*, 5318.

[35] C. DeSantis, J. Ma, L. Bryan, A. Jemal, *CA Cancer J Clin* **2014**, *64*, 52.

[36] S. A. Hosseini-Yazdi, A. Mirzaahmadi, A. A. Khandar, V. Eigner, M. Dušek, M. Mahdavi, J. White, *Polyhedron* **2017**, *124*, 156.

[37] P. Kumar, B. Narasimhan, K. Ramasamy, V. Mani, R. K. Mishra, A. B. A. Majeed, *Curr. Top. Med. Chem.* **2015**, *15* (11), 1050.

[38] D. J. Majumdar, S. Das, J. K. Biswas, M. Mondal, *J. Mol. Struct.* **2017**, *1134*, 617.

[39] D. J. Majumdar, J. K. Biswas, M. Mondal, M. S. Surendra Babu, R. K. Metre, S. Das, K. Bankura, D. Mishra, *J. Mol. Struct.* **2018**, *1155*, 745.

[40] D. J. Majumdar, J. K. Biswas, M. Mondal, M. S. Surendra Babu, S. Das, R. K. Metre, S. S. SreeKumar, K. Bankura, D. Mishra, *ChemistrySelect,* **2018,** *3*, 2912–2925.

[41] D. J. Majumdar, S. Dey, S. S. Sreekumar, S. Das, D. Das, R. K. Metre, K. Bankura, D. Mishra, *ChemistrySelect* **2018**, *3*, 12371.

[42] D. J. Majumdar, D. Das, S. S. Sreejith, S. Das, J. K. Biswas, M. Mondal, D. Ghosh, K. Bankura, D. Mishra, *Inorg. Chim. Acta*. **2019**, *489*, 244. https://doi.org/10.1016/j.ica.2019.02.022

[43] S. Ponsico, H. Gulyas, M. Martnez-Belmonte, E. C. Escudero-Adan, Z. Freixa, P. W. N. M. van Leeuwen, *Dalton Trans* **2011**, *40*, 10686.

[44] H. Wang, D. Zhang, Z. -H. Ni, X. Li, L. Tian, J. Jiang, *Inorg. Chem.* **2009**, *48*, 5946.

[45] Z. -L. You, Y. Lu, N. Zhang, B.-W. Ding, H. Sun, P. Hou, C. Wang, *Polyhedron* **2011**, *30*, 2186.

[46] Y.-N. Guo, *Synth. React. Inorg., Met.-Org., Nano-Met. Chem.* **2011**, *41*, 987.

[47] L. K. Das, S. -W. Park, S. J. Cho, A. Ghosh, *Dalton Trans* **2012**, *41*, 11009.

[48] S. Konar, *J. Mol. Struct.* **2015**, *1092*, 34.

[49] J. Kohout, L. Jager, M. Hvastijova, J. Kozısek, *J. Coord. Chem.* **2000**, *51*, 169.

[50] J. S. Miller, J. L. Manson, *Acc. Chem. Res.* **2001**, *34*, 563.

[51] S. R. Batten, K. S. Murray, *Coord. Chem. Rev.* **2003**, *246*, 103.

[52] I. Potoncak, M. -J. Dunaj, D. M. Miklos, L. Jager, *Acta Crystallogr Sect C* **1996**, *52*(52), 1653.

[53] J. L. Manson, C. D. Incarvito, A. L. Rheingold, J. S. J. Miller, *Chem Soc, Dalton Trans* **1998**, 2552.

[54] J. L. Manson, C. R. Kmety, Q. Huang, J. W. Lynn, G. Bendele, S. Pagola, P. W. Stephens, L. M. –. S. Liabe, A. L. Rheingold, A. J. Epstein, J. S. Miller, *Chem. Mater.* **1998**, *10*, 2552.

[55] Y. M. Chow, D. Britton, *Acta Crystallogr Sec C* **1975**, *37*, 1934.

[56] D. R. Turner, A. S. R. Chesman, K. S. Murray, G. B. Deacon, S. R. Batten, *Chem Commun* **2011**, *47*, 10189.

[57] D. J. Majumdar, S. Das, R. Thomas, Z. Ullah, S. S. Sreejith, D. Das, P. Shukla, K. Bankura, D. Mishra, **2019**, 492, 221. https://doi.org/10.1016/j.ica.2019.04.041

[58] B. Valeur, *Molecular Fluorescence, Principles and Applications*, Fifth ed., Wiley-VCH, Wienheim **2009** 161.

[59] S. Thakurta, C. Rizzoli, R. J. Butcher, C. J. Gomez-Garcia, E. Garribba, S. Mitra, *Inorg. Chim. Acta* **2010**, *363*, 1395.

[60] G. M. Sheldrick, *SADABS*, a software for empirical absorption correction*, Ver. 2.05*, University of Göttingen, Göttingen **2002**.

[61] SMART & SAINT, *Software Reference manuals, Version 6.45*, Bruker Analytical X-ray Systems, Inc, Madison, WI **2003**.

[62] SHELXTL, *Reference Manual, Ver. 6.1*, Bruker Analytical X-ray Systems, Inc, Madison, WI **2000**.

[63] G. M. Sheldrick, *SHELXTL,* a software for empirical absorption correction *Ver.6.12*, Bruker AXS Inc., Madison, WI **2001**.

[64] O. V. Dolomanov, L. J. Bourhis, R. J. Gildea, J. A. K. Howard, H. Puschmann, *J Appl Crystallog* **2009**, *42*, 339.

[65] K. Bradenburg, *Diamond, Ver. 3.1eM*, Crystal Impact GbR, Bonn **2005**.

[66] M. J. Frisch, G. W. Trucks, H. B. Schlegel, G. E. Scuseria, M. A. Robb, J. R. Cheeseman, G. Scalmani, V. Barone, B.

Mennucci, G. A. Petersson, H. Nakatsuji, M. Caricato, X. Li, H. P. Hratchian, A. F. Izmaylov, J. Bloino, G. Zheng, J. L. Sonnenberg, M. Hada, M. Ehara, K. Toyota, R. Fukuda, J. Hasegawa, M. Ishida, T. Nakajima, Y. Honda, O. Kitao, H. Nakai, T. Vreven, J. A. Montgomery Jr., J. E. Peralta, F. Ogliaro, M. Bearpark, J. J. Heyd, E. Brothers, K. N. Kudin, V. N. Staroverov, T. Keith, R. Kobayashi, J. Normand, K. Raghavachari, A. Rendell, J. C. Burant, S. S. Iyengar, J. Tomasi, M. Cossi, N. Rega, J. M. Millam, M. Klene, J. E. Knox, J. B. Cross, V. Bakken, C. Adamo, J. Jaramillo, R. Gomperts, R. E. Stratmann, O. Yazyev, A. J. Austin, R. Cammi, C. Pomelli, J. W. Ochterski, R. L. Martin, K. Morokuma, V. G. Zakrzewski, G. A. Voth, P. Salvador, J. J. Dannenberg, S. Dapprich, A. D. Daniels, O. Farkas, J. B. Foresman, J. V. Ortiz, J. Cioslowski, D. J. Fox, *Gaussian 09, (Revision D.0)*, Gaussian, Inc., Wallingford, CT **2010**.

[67] R. Dennington, T. Keith, J. Millam, *Gauss view, Version 5*, Semichem Inc., Shawnee Mission, KS **2009**.

[68] M. J. Turner, J. J. McKinnon, S. K. Wolff, D. J. Grimwood, P. R. Spackman, D. Jayatilaka, M. A. Spackman, *Crystal Explorer 17* (**2017**). University of Western Australia. http://hirshfeldsurface.net.

[69] S. P. Cole, *Cancer Chemother Pharmacol* **1986**, *17*, 259.

[70] M. K. Santra, N. Wajapeyee, M. R. Green, *Nature* **2009**, *459*, 722.

[71] M. M. Bradford, *Anal. Biochem.* **1976**, *72*, 248.

[72] M. Herrmann, H. M. Lorenz, R. Voll, M. Grünke, W. Woith, J. R. Kalden, *Nucleic Acids Res.* **1994**, *22*, 5506.

[73] M. Maiti, S. Thakurta, D. Sadhukhan, G. Pilet, G. M. Rosair, A. Nonat, L. J. Charbonniere, S. Mitra, *Polyhedron* **2013**, *65*, 6.

[74] M. T. H. Tarafder, A. Kasbollah, K. A. Crouse, A. M. Ali, B. M. Yamin, H. K. Fun, *Polyhedron* **2001**, *20*, 2363.

[75] S. H. Rahaman, R. Ghosh, T. -H. Lu, B. K. Ghosh, *Polyhedron* **2005**, *24*, 1525.

[76] K. Nakamoto, *Infrared and Raman Spectra of Inorganic and Coordination Compounds, Theory and Applications in Inorganic Chemistry*, 5th ed., John Wiley and Sons, Inc., New York **1997**.

[77] H. Kohler, A. Kolbe, G. Lux, *Z Allg Chem* **1977**, *428*, 103.

[78] W. K. Dong, Y. X. Sun, C. Y. Zhao, X. Y. Dong, L. Xu, *Polyhedron* **2010**, *29*, 2087.

[79] A. B. P. Lever, *Inorganic Spectroscopy*, Second ed., Elsevier, New York **1984**.

[80] A. Roy, D. Sadhukhan, G. M. Rosair, C. J. Gomez-Garcia, S. Mitra, *Polyhedron* **2009**, *28*, 3542.

[81] G. B. Furman, A. M. Panich, A. Yochelis, E. M. Kunoff, S. D. Goren, *Phys. Rev. B* **1997**, *55*, 439.

[82] Q. Shi, L. Sheng, K. Ma, Y. Sun, X. Cai, R. Liu, S. Wang, *Inorg. Chem. Commun.* **2009**, *12*, 255.

[83] A. W. Addison, T. N. Rao, J. Reedijk, J. V. Rijn, G. C. Verschoor, *J Chem Soc Dalton Trans* **1984**, 1349.

[84] C. Maxim, T. D. Pasatoiu, V. C. Kravtsov, S. Shova, C. A. Muryn, R. E. P. Winpenny, F. Tuna, M. Andhruh, *Inorg. Chim. Acta* **2008**, *361*, 3903.

[85] M. Maiti, S. Thakurta, D. Sadhukhan, S. Roy, G. Pilet, G. M. Rosair, A. Nonat, L. J. Charbonniere, R. J. Butcher, S. Mitra, *Inorg. Chem.* **2012**, *51*, 12176.

[86] J. J. McKinnon, A. S. Mitchell, M. A. Spackman, *Chem - a Eur J* **1998**, *4*(11), 2136.

[87] R. G. Parr, R. G. Pearson, *J. Am. Chem. Soc.* **1983**, *105*, 7512.

[88] F. A. Bulat, A. Toro-Labbé, T. Brinck, J. S. Murray, P. Politzer, *J. Mol. Model.* **2010**, *16*, 1679.

[89] J. He, Y. -G. Yin, X. -C. Huang, D. Li, *Inorg. Chem. Commun.* **2006**, *9*, 205.

[90] J. R. Lakowicz, *Topics in Flourescence Spectroscopy*, Plenum Press, New York **1994**.

[91] S. Ray, S. Konar, A. Jana, S. Patra, S. Chatterjee, J. A. Golen, A. L. Rheingold, S. Mandal, S. K. Kar, *Polyhedron* **2012**, *33*, 82.

[92] Y. Li, L. Shi, L.-X. Qin, L.-L. Qu, C. Jing, M. Lan, T. D. James, Y. -T. Long, *Chem Commun* **2011**, *47*, 4361.

[93] A. Valek Jr., *Coord. Chem. Rev.* **2000**, *200*, 933.

[94] D. -W. Fu, H. -L. Cai, Y. Liu, Q. Ye, W. Zhang, Y. Zhang, X. -Y. Chen, G. Giovannetti, M. Capone, J. Li, R. -G. Xiong, *Science* **2013**, *339*, 425.

[95] D. -W. Fu, W. Zhang, H. -L. Cai, Y. Zhang, J. -Z. Ge, R. -G. Xiong, S. D. Huang, *J. Am. Chem. Soc.* **2011**, *133*, 12780.

[96] D. -W. Fu, W. Zhang, H. -L. Cai, J. -Z. Ge, Y. Zhang, R. -G. Xiong, *Adv. Mater.* **2011**, *23*, 5658.

[97] D. -W. Fu, H. -L. Cai, S. -H. Li, Q. Ye, L. Zhou, Y. Zhang, F. Deng, R. -G. Xiong, *Phys. Rev. Lett.* **2013**, *110*, 257601.

[98] W. -Y. Zhang, Y. -Y. Tang, P. -F. Li, P.-P. Shi, W. -Q. Liao, D. -W. Fu, H. -Y. Ye, Y. Zhang, R. -G. Xiong, *J. Am. Chem. Soc.* **2017**, *139*, 10897.

[99] M. Formica, V. Fusi, L. Giorgi, M. Mcheoni, *Coord. Chem. Rev.* **2012**, *356*, 170.

[100] Z. Wang, J. Wang, J. Li, M. Feng, G. Zou, X. Huang, *Chem Commun* **2015**, *51*, 3094.

[101] K. Takahashi, Y. Hasegawa, R. Sakamoto, M. Nishikawa, S. Kume, E. Nishibori, H. Nishihara, *Inorg. Chem.* **2012**, *51*, 5188.

[102] P. Ghosh, P. K. Bharadwaj, J. Roy, S. Ghosh, *J. Am. Chem. Soc.* **1997**, *119*, 11903.

[103] N. Dwivedi, S. S. Sunkari, A. Verma, S. Saha, *Cryst. Growth des.* **2018**, *18*(9), 5628.

[104] I. Majumder, P. Chakraborty, S. Dasgupta, C. Massera, D. Escuredero, D. Das, *Inorg. Chem.* **2017**, *56*(21), 12893.

[105] P. Chakraborty, J. Adhikary, S. Samanta, D. Escudero, A. C. Castro, M. Swart, S. Ghosh, A. Bauzá, A. Frontera, E. Zangrando, D. Das, *Cryst. Growth des.* **2014**, *14*(8), 4111.

[106] N. Muhammd, N. Sadia, C. Zhu, C. Luo, Z. Guo, X. Wang, *Chem Commun* **2017**, *53*, 9971.

[107] U. M. Rafi, D. Mahendiran, A. K. Haleel, R. P. Nankar, M. Doble, A. K. Rahiman, *New J. Chem.* **2016**, *40*, 2451.

[108] L. N. Pluchino, S. Choudhury, H. -C. Robert Wang, *Cancer Lett.* **2016**, *381*, 124.

[109] J. Devi, M. Yadav, D. K. Jindal, D. Kumar, Y. Poornachandra, *Appl Organometal Chem*. **2019**, e5154.https://doi.org/10.1002/aoc.5154.

[110] https://doi.org/10.1002/aoc.4693.

[111] https://doi.org/10.1002/aoc.3542.

[112] https://doi.org/10.1039/c9nj01814j.

[113] https//doi.org/10.1002/aoc.3776

[114] https//doi.org/10.1002/aoc.4753

[115] https://doi.org/10.1016/j.jinorgbio.2019.110790.

[116] https://doi.org/10.1086/1471-2407-14-73.

[117] E. Narvi, K. Jaakkola, S. Winsel, C. O. Lindholm, P. Halonen, L. Kallio, M. J. Kallio, J. British, *Cancer* **2013**, *108*, 179.

[118] C. Balakrishnan, M. Theetharappan, P. Kowsalya, S. Natarajan, M. A. Neelakantan, S. S. Mariappan, *Appl Organometal Chem* **2017**, *31*, 3776.

[119] G. Kroemer, *Cell Death Differ* **2005**, *12*, 1463.

[120] Q. Chen, J. Kang, C. Fu, *Signal Transduction Targeted Ther.* **2018**, *3*, 18.

SUPPORTING INFORMATION

Additional supporting information may be found online in the Supporting Information section at the end of the article.

How to cite this article: Majumdar D, Agrawal Y, Thomas R, et al. Syntheses, characterizations, crystal structures, DFT/TD-DFT, luminescence behaviors and cytotoxic effect of bicompartmental Zn (II)-dicyanamide Schiff base coordination polymers: An approach to apoptosis, autophagy and necrosis type classical cell death. *Appl Organometal Chem*. 2019;e5269. https://doi.org/10.1002/aoc.5269